Reactions of Aluminum Oxide Cluster Cations with Ethane: A Mass-Spectrometric and Vibrational Spectroscopy Study

Apakorn Phasuk and Prof. Ricardo B. Metz*
Department of Chemistry, University of Massachusetts Amherst, Amherst, Massachusetts 01003, United States
rbmetz@chem.umass.edu

Published in *ChemPhysChem*, 2024 e202400427 (18 pgs.)
DOI: 10.1002/cphc.202400427
For version of record, please see https://doi.org/10.1002/cphc.202400427

Abstract

The pathways for the reactions of aluminum oxide cluster ions with ethane have been measured. For selected ions (Al_2O^+, $Al_3O_2^+$, $Al_3O_4^+$, $Al_4O_7^+$) the structure of the collisionally-stabilized reaction intermediates were explored by measuring the photodissociation vibrational spectra from 2600 cm^{-1} to 3100 cm^{-1}. Density functional theory was used to calculate features of the potential energy surfaces for the reactions and the vibrational spectra of intermediates. Generally, more than one isomer contributes to the observed spectrum. The oxygen-deficient clusters Al_2O^+ and $Al_3O_2^+$ have large C-H activation barriers, so only the entrance channel complexes in which intact C_2H_6 binds to aluminum are observed. This interaction leads to a substantial (~200 cm^{-1}) red shift of the C-H symmetric stretch in ethane, indicating significant weakening of the proximal C-H bonds. In $Al_3O_4^+$, the complex formed by interactions with three C_2H_6 is investigated and, in addition to entrance channel complexes, the C-H activation intermediate $Al_3O_4H^+(C_2H_5)(C_2H_6)_2$ is observed. For oxygen-rich $Al_4O_7^+$, the C_2H_6 is favored to bind at an aluminum site far from the reactive superoxide group, reducing the reactivity. As expected, oxygen-rich species and open-shell cluster ions have smaller barriers for C-H bond activation, except for $Al_3O_4^+$ which is predicted and observed to be reactive.

I. Introduction

Metal-containing clusters and their reactions with hydrocarbons have been widely studied to gain fundamental understanding of the underlying chemistry and to advance the development of new applications.[1,2] One application is the enhancement of jet engine performance by increasing thrust using metal-containing clusters as a fuel additive and catalyst to accelerate combustion.[3] In this application, a major goal is for the catalyst to facilitate C-H bond activation,[4–6] which typically has a large barrier, followed by hydrogen atom transfer (HAT) to form radical species. In this process, the hydrogen atom of the fuel is abstracted by the catalyst, producing a hydrocarbon radical that reacts much more rapidly with oxygen than the non-activated hydrocarbon.[7] The maximum rate constant for gas-phase ion-molecule reactions is a factor of ten higher than for analogous neutral species. This is because the stronger and longer-range attractive ion-dipole/induced dipole intermolecular forces increase the collision rate.[8] Therefore, even a small concentration of ions could affect the course of a combustion reaction network, because the ions react so much faster than the neutrals. Metal oxides are well known as catalysts for C-H bond activation. In addition to accelerating combustion by increasing the oxidation of hydrocarbons, they can also act as an oxygen buffer against NO_x formation.[9]

Numerous recent works have studied C-H bond activation of small alkanes by various gas-phase metal oxide clusters in both cationic and anionic forms.[1] Some especially well-studied systems include FeO^+,[10] $(MoO_3)_{1\text{-}2}^+$,[11] GeO^+, SnO^+, PbO^+,[12] MgO^+,[13] $Al_2O_2^+$,[14] $Al_2O_7^+$,[7] $(Al_2O_3)_x^+$,[15] $Zr_2O_8^-$,[16] and $Sc_3O_6^-$.[17] Despite the fact that catalysts are mostly based on transition metal-containing compounds due to their high reactivity, their drawbacks may include toxicity, high cost, and low availability in nature. Hence, the development of alternative catalysts based on main-group metals such as Mg and Al is attractive. Aluminum and aluminum oxides are used as catalysts in reactions involving breaking a C-H bond, such as combustion, H/D exchange, and hydrogen atom transfer (HAT).[7,9,18–21]

Aluminum and its cluster cations react readily with oxygen, and the product clusters often react rapidly with hydrocarbons. A study by Biswas et al. on the decomposition and oxidation of $C_{10}H_{16}$ (JP-10) in the presence of aluminum oxide (Al_2O_3)-coated aluminum nanoparticles (AlNPs) reveals that the product branching ratio is temperature dependent.[22] Oxygenated products dominate at low temperatures via reaction with oxide layers, whereas hydrocarbons and their radicals dominate at high temperatures via the reaction with AlO. Upon ignition of Al/CuO

nanoparticles, Al^+ is formed; Al_2O^+ is also observed following electron impact ionization of gas-phase species formed by ignition Al and mixed Al/metal oxide nanoparticles.[23,24] However, bulk catalysts are complex, and their structures at the molecular scale remain difficult to characterize and predict.[25] A promising way to study the reactions of metal oxides is to generate gas-phase metal oxide clusters and investigate their chemical reactivity with small alkanes, which allows us to build the mechanism of C-H activation from results on "small" clusters with <10 Al atoms with known composition and extend this knowledge to the mechanism for nanoparticles with thousands of atoms.[7]

To improve the activity of aluminum oxide clusters as fuel additives, it is important to understand their structure and the complex interactions between the clusters and fuels. The structures of neutral aluminum oxide clusters have been studied using vibrational spectroscopy at free-electron lasers (FEL)[25] by Sierka et al.[26] and van Heijnsbergen et al.,[27] while Song et al.[28] studied anionic clusters and Sierka et al.,[26] Santambrogio et al.[29] and Kiawi et al.[30] studied the cationic clusters. Based on gas-phase IR spectroscopy, the neutral[27] and some cationic[30] clusters adopt structures similar to the γ-Al_2O_3 bulk phase. However, cationic $AlO^+(Al_2O_3)_n$ (n=1-4) clusters have more highly symmetrical structures.[29]

There have been several gas-phase studies of the reactions of aluminum oxide cations with methane, which is both the simplest stable hydrocarbon and one with particularly strong C-H bonds. In 2008, the first thermal activation of methane by a polynuclear main group metal oxide cluster, $(Al_2O_3)_x^+$, was reported by Schwarz and coworkers.[15] In 2011, the same group observed that $Al_2O_7^+$ also activates methane, and in 2017, they showed that $Al_2O_2^+$ is the smallest aluminum oxide cluster that activates methane.[7,31] Recently, Shuman et al. measured temperature-dependent kinetics of the reactions of several aluminum oxide cluster cations with methane and ethane.[32] Their results will be discussed in more detail below. However, our understanding of the mechanisms, kinetics and (especially) the structures of the intermediates and products of the reactions of aluminum oxide clusters with fuel molecules is still lacking, even for simple cases like small hydrocarbons.[33]

Schwarz and coworkers described different types of methane activation mechanisms by metal oxide cluster ions. They include H-atom transfer, oxygen-atom transfer, carbene and formaldehyde formation:[5,6,34,35]

$[(M_xO_y)O]^+ + CH_4 \rightarrow [(M_xO_y)OH]^+ + CH_3\cdot$ H-atom transfer

$[(M_xO_y)O]^+ + CH_4 \rightarrow [M_xO_y]^+ + CH_3OH$ Oxygen-atom transfer

$[(M_xO_y)O]^+ + CH_4 \rightarrow [(M_xO_y)CH_2]^+ + H_2O$ Carbene formation

$[(M_xO_y)O]^+ + CH_4 \rightarrow [M_xO_yH_2]^+ + CH_2O$ Formaldehyde formation

Only H-atom transfer and formaldehyde formation have been observed for aluminum oxide cluster ions, with oxygen-rich clusters favoring formaldehyde formation.[7,36]

Jet fuel consists of mixed C5-C16 hydrocarbons and is used to power gas-turbine engines in aircraft.[37] Therefore, molecules larger than methane are a better model for jet fuel, and there are very few studies on these larger hydrocarbons. Ethane has weaker C-H bonds than methane, so it should be more reactive towards metal oxide cluster ions.[35] In addition, metal oxides can react with alkanes larger than methane to form alkenes via double H-atom transfer[38,39]

$[(M_xO_y)O]^+ + C_nH_{2n+2} \rightarrow [(M_xO_{y-1})(OH)_2]^+ + C_nH_{2n}$ Double H-atom transfer

The first intermediate in these reactions is an entrance channel complex - an adduct between the cation and hydrocarbon. However, many additional intermediates are formed in the course of these reactions, and the stability of the intermediates can affect the preferred reaction pathway.[40]

Here, we use a fast-flow reactor source to measure coarse kinetics for the reactions between aluminum oxide cations and ethane as a representative aliphatic hydrocarbon and infrared multiple photon photodissociation spectroscopy, to obtain vibrational information on cluster cations by using a mass spectrometer. to gain insight into the structures of the intermediates and products of the reactions and to establish a model to understand the C – H bond activation mechanism.

II. Experimental and Computational Methods

A home-build laser ablation dual time-of-flight reflectron mass spectrometer was used in these studies.[41] The cluster ions are produced using a two-valve fast flow reactor source that is based on the design of Rothgeb et al.,[42] is described in detail in Kozubal et al.[43] and is shown in Figure S1. Aluminum oxide cations are produced and thermalized to ~300 K in the first region and then react with ethane introduced in the second region. Ions are produced by ablating an aluminum rod with the frequency-doubled 532 nm output of a Nd:YAG laser operating at 20 Hz and 9 mJ/pulse. The primary pulsed valve introduces a gas mixture of 0.4 to 1.6% O_2 and 0 to 20% Ar in He at a backing pressure of 20 psi which interacts with the resulting plasma in the first section

of the fast flow reactor, producing $Al_xO_y^+$ ions, where x = 2–5, y = 1–10. The optimized conditions for each type of $Al_xO_y^+$ cluster ion are obtained by varying the percentage of O_2 and the backing pressure. Then the cluster ions undergo reaction with C_2H_6 introduced via the secondary valve to make product ions, including $Al_xO_y^+(C_2H_6)_n$ and $Al_xO_yH_z^+$. The secondary gas consists of 0.02% to 3.3% C_2H_6 in He at a backing pressure of 20 to 40 psi. In some cases it is desirable to measure vibrational spectra of N_2-tagged ions. They are produced using a primary gas mixture of 0.4 to 1.6% O_2 and 20% N_2 in He at 20 psi.

Ions formed in the source undergo a supersonic expansion into vacuum, cooling to a rotational temperture of ~15 K.[44] The vibrational temperature is higher. The ions are then injected into a reflectron time-of-flight mass spectrometer. The relative reactivities of $Al_xO_y^+$ with ethane and subsequent reaction products are determined by measuring mass spectra with the secondary valve on and off. The vibrational spectra of ions of interest are measured using photofragment spectroscopy. If the photodissociation quantum yield is one (or is constant across the spectrum), which is typically the case, then the photodissociation spectrum mirrors the absorption spectrum. Some of the ions studied have a sufficiently low binding energy that they dissociate after absorption of one IR photon. Spectra of more strongly bound ions are measured via infrared multiple-photon dissociation (IRMPD), which is more efficient for the larger clusters, due to their high rate of intramolecular vibrational energy redistribution (IVR) or by tagging the ion of interest with a weakly bound molecule such as N_2.

The mass-selected ions are irradiated at the turning point of the reflectron by a pulse of IR light. The light is multipassed[45] to increase the dissociation yield, which is especially effective for IRMPD. The IR laser system is a Nd:YAG pumped optical parametric oscillator/optical parametric amplifier which produces about 6 mJ/pulse near 3100 cm^{-1} and is tunable from 2500 to >4000 cm^{-1}. The wavenumber is calibrated using the absorption spectrum of methane.[46] The parent and fragment ions are mass analyzed in the second time-of-flight region. The vibrational spectra are collected by monitoring fragment ion intensity as a function of IR wavenumber and normalizing to parent ion intensity and laser power.

To determine the structures of the reaction products and investigate their bonding, the optimized geometries of possible isomers and their vibrational spectra are calculated with the *Gaussian09* program package.[47] Calculations are carried out at the B3LYP/TZVP, B3LYP/6-311+G(d,p), B3LYP+D3/6-311+G(d,p) and ωB97X-D/6-311+G(d,p) levels of theory to get

information on geometries, energies, and harmonic vibrational frequencies. All reported energies include zero-point energy. The vibrational frequencies from the B3LYP/TZVP level of theory are scaled by a factor of 0.965 based on the ratio of experimental and calculated C–H stretching frequencies in ethane. In addition, anharmonic effects and the contribution of C–H bending overtones and combination bands are included using the local mode Hamiltonian (LMH) approach of Sibert and coworkers[48,49] with the B3LYP/6-311+G(d,p), B3LYP+D3/6-311+G(d,p) and ωB97X-D/6-311+G(d,p) levels of theory. The scaling factors and anharmonic couplings are based on alkyl benzenes and were not adjusted in this study. All simulated spectra are generated by convoluting the calculated stick spectrum with a Gaussian with 20 cm^{-1} fwhm.

III. Results and Discussion

III. A. Overview of reactions

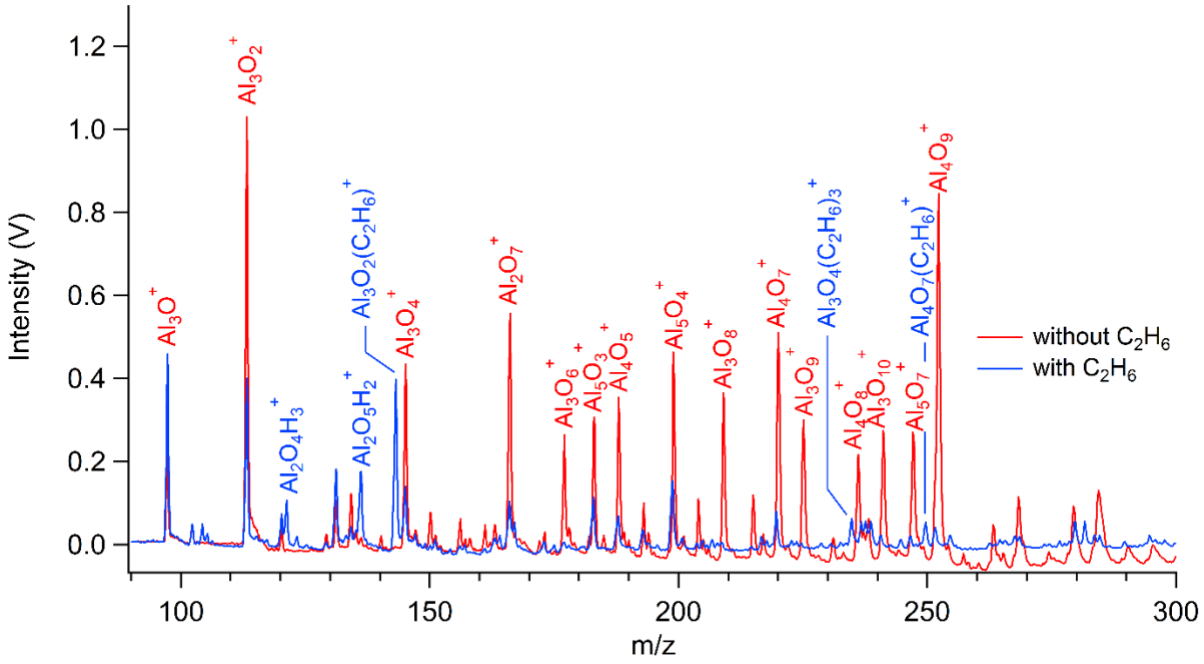

Figure 1. Mass spectrum of $Al_xO_y^+$ using 0.75% O_2 in He in the primary valve (red) and reaction products of $Al_xO_y^+$ formed by introducing 0.8% C_2H_6 in He in the secondary valve (blue).

Figure 1 shows the mass spectrum obtained by ablating aluminum in a pulse of O_2 in He, along with the mass spectrum obtained when C_2H_6 in He is introduced via the secondary valve. Focusing first on the results with the primary valve alone, the $Al_xO_y^+$ product distribution depends

on O_2 concentration, as shown in detail in Fig. S2. Results for $Al_2O_y^+$, $Al_3O_y^+$, and $Al_4O_y^+$ are broken out in Figs. S3-S5. At low O_2 concentration, $Al_3O_2^+$ and $Al_4O_7^+$ are the dominant species. Oxygen-rich species, $Al_2O_7^+$, $Al_3O_9^+$ and $Al_4O_9^+$, are the main cluster products at high O_2 concentrations, which is in agreement with the results reported by the Khanna group.[50] The product distributions are as expected, since at lower O_2 concentration, the Al to O ratio is high, leading to the formation of oxygen-poor clusters and vice versa for higher O_2 concentration. However, if the O_2 level is too high or low, all signals for small clusters drop dramatically. This may be due to rapid cluster growth at high [O_2], forming only large clusters, or lacking enough O_2 to form clusters at all at low [O_2]. These results confirm that O_2 concentration plays a crucial role in regulating $Al_xO_y^+$ products, and allows us to select the [O_2] to optimize production of each cluster of interest.

The fast-flow reactor allows us to vary the C_2H_6 concentration via the secondary valve and to study the rough kinetics of reactions of $Al_xO_y^+$ with ethane. The kinetics are qualitative, not quantitative, as the neutral concentration is not accurately known, and the pressure is fairly high, so adducts and other reaction intermediates can be stabilized and primary products can react further to form secondary products. As shown in Fig. 1, when ethane is introduced, the signal of most $Al_xO_y^+$ drops, with some ions dropping by >90%. New ions are formed, and they are of two general types: $Al_xO_yH_n^+$ formed by hydrogen abstraction and $Al_xO_y^+(C_2H_6)_n$ adducts or reaction intermediates. Based on multiple experiments with differing O_2 and C_2H_6 concentrations, the observed reactions are shown in Scheme 1. The observed reactions suggested that the oxygen rich clusters tend to release O_2 and become smaller clusters. $Al_2O_y^+$ abstracts the H atom from ethane to form the reaction product $Al_2O_yH^+$, implying high C-H bond activation reactivity. Meanwhile, $Al_3O_y^+$ and $Al_4O_y^+$ mostly form an association product with ethane. However, from the mass spectrum, we cannot identify whether the ethane is intact or we activate the C–H bond.

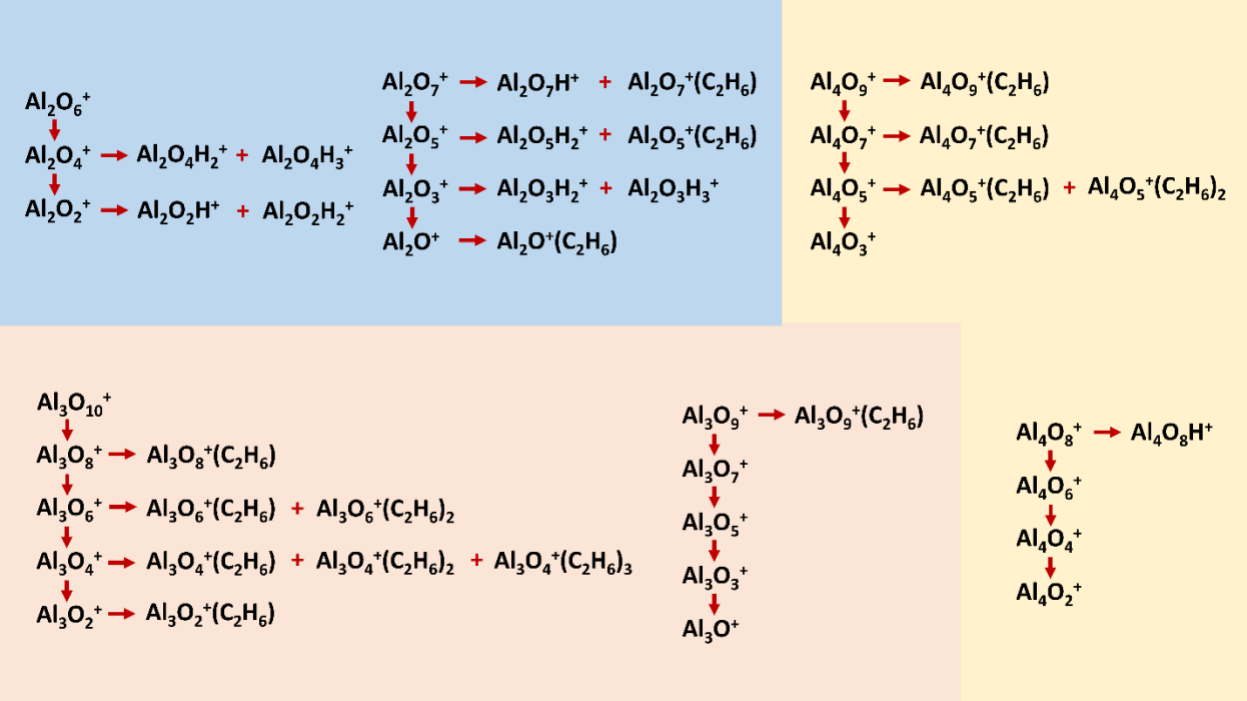

Scheme 1. Observed reactions of $Al_xO_y^+$ with C_2H_6

The oxygen-rich clusters $Al_2O_y^+$, $Al_3O_y^+$ and $Al_4O_y^+$ (y = 6-9), tend to lose O_2. $Al_2O_5^+$, $Al_2O_7^+$, $Al_3O_2^+$(outstanding), $Al_3O_4^+$, $Al_3O_6^+$, $Al_3O_7^+$, $Al_3O_9^+$, $Al_4O_5^+$, $Al_4O_7^+$ and $Al_4O_9^+$ form adducts with C_2H_6. Meanwhile, $Al_2O_4^+$, $Al_2O_5^+$ (outstanding) and $Al_2O_7^+$ abstract hydrogen atom(s) from C_2H_6, which implies that these $Al_xO_y^+$ species, all of which have an even number of aluminum atoms, have higher C-H bond activation reactivities than the other clusters.

Previous studies have identified the key factors that predict the reactivity of $Al_xO_y^+$ with methane[6,51] and are expected to apply to reactions with other aliphatic hydrocarbons. $Al_xO_y^+$ with an odd number of Al have an even number of electrons, are closed shell, and are the least reactive. Those with an even number of Al have one unpaired electron. If the cluster has a non-bridging oxygen, the unpaired electron tends to be localized on this oxygen, and these are the most reactive clusters, with the oxygen abstracting a hydrogen from the hydrocarbon. These results correlate with the energy calculations in Table 1, $Al_xO_y^+$ with an even number of Al tend to have products which are lower in energy and reactions that are more exothermic than $Al_xO_y^+$ with an odd number of Al. In addition, hydrogen abstraction by $Al_2O_3^+$, which has an non-bridging oxygen, is more exothermic than for $Al_2O_2^+$. Furthermore, the $Al_xO_y^+$ with an even number of Al also tend to have

lower activation energy, especially for the second C-H activation. $Al_2O_3^+$ is remarkable in that there is not even a submerged barrier to the first C-H activation, hence it is expected to react more rapidly than the other clusters in this study.

Schwarz and coworkers have extensively studied the reactions of $Al_xO_y^+$ with methane, observing reactions with $Al_2O_2^+$,[14] $Al_2O_3^+$,[7] $Al_2O_7^+$,[7] and $(Al_2O_3)_x^+$.[15] In each case, they found that H-atom transfer from the methane to the aluminum oxide cluster occurs via oxygen centered radical species. As we discussed above, aluminum oxide cluster cations with an odd number of aluminum atom showed no reaction with methane due to their lack of an oxygen-centered radical.[15]

Table 1. Bond dissociation energies and relative energies of $Al_2O_2^+$, $Al_2O_3^+$, $Al_3O_2^+$, and $Al_3O_4^+$ + C_2H_6 systems calculated at the B3LYP/TZVP level of theory.

Species	E_{rel}(kJ/mol)	Species	E_{rel}(kJ/mol)
$Al_2O_2^+ + C_2H_6$	0	$Al_3O_2^+ + C_2H_6$	0
TS1/E_a	-2.1/112.3	TS1/E_a	86.7/126.9
$Al_2O_2H^+ + C_2H_5$	-60.5	$Al_3O_2H^+ + C_2H_5$	255.4
TS2/E_a	-115.3/160.7	TS2/E_a	246.6/289.6
$Al_2O_2H_2^+ + C_2H_4$	-136.7	$Al_3O_2H_2^+ + C_2H_4$	202.7
$Al_2O_3^+ + C_2H_6$	0	$Al_3O_4^+ + C_2H_6$	0
TS1/E_a	NA[a]	TS1/E_a	-12.8/96
$Al_2O_3H^+ + C_2H_5$	-119.5	$Al_3O_4H^+ + C_2H_5$	-25.6
TS2/E_a	-232.6/108.2	TS2/E_a	-93.4/238.4
$Al_2O_3H_2^+ + C_2H_4$	-395.4	$Al_3O_4H_2^+ + C_2H_4$	-218.7

E_a is the activation energy relative to the previous minimum. Potential energy surfaces are Fig. S6–S9.

[a] the reaction is barrierless.

III. B. Vibrational spectra

III. B. 1. Overview

In order to determine whether some of the observed $Al_xO_y^+(C_2H_6)_n$ ions are adducts with intact ethanes, or are stabilized reaction intermediates that have undergone C-H bond activation, we measured vibrational spectra of selected ions. We did not measure vibrational spectra of hydrogen abstraction products $Al_xO_yH_n^+$ because only the O-H stretches are in the range of our laser system, and they are not very diagnostic of different structural isomers, without additional spectra in the fingerprint region.[52] Also, they have strong covalent bonds, which makes fragmentation challenging or requires tagging. In addition, vibrational spectra can only be measured for the most abundant ions, due to signal to noise considerations. As a result, we are unable to measure spectra of product ions of some of the most reactive clusters, such as $Al_2O_2^+$ and $Al_2O_3^+$. We will discuss the potential energy surfaces for the reactions of Al_2O^+, $Al_3O_2^+$, $Al_3O_4^+$ and $Al_4O_7^+$ with ethane, and the structure and vibrational spectra of the corresponding ions $Al_2O^+(C_2H_6)$, $Al_3O_2^+(C_2H_6)$, $Al_3O_2^+(C_2H_6)(N_2)$, $Al_3O_4^+(C_2H_6)_3$ and $Al_4O_7^+(C_2H_6)$.

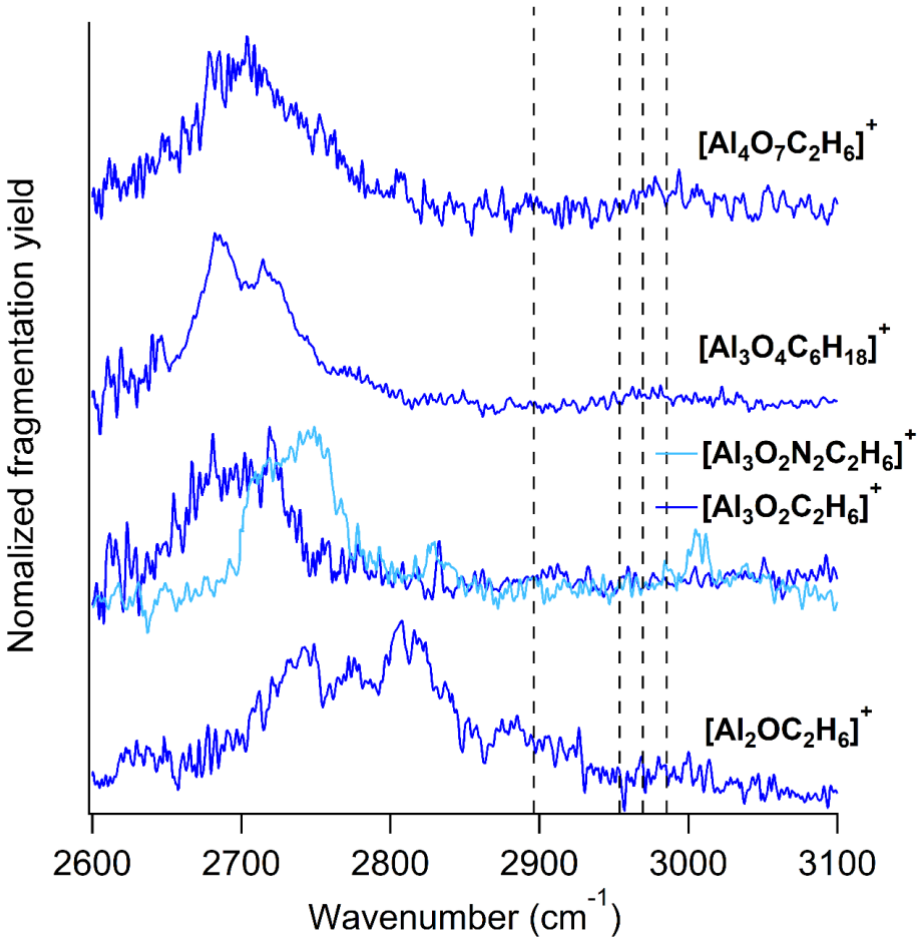

Figure 2. Vibrational spectra of key $Al_xO_y^+(C_2H_6)_n(N_2)_k$, in the C-H stretching region (2600-3100 cm^{-1}). The experimental positions of the symmetric and antisymmetric C-H stretches in C_2H_6 are shown with dashed lines.

The vibrational spectra of several $Al_xO_y^+(C_2H_6)_n(N_2)_k$ are shown in Figure 2. All of the intense peaks are below 2850 cm^{-1} and most are near 2700 cm^{-1}. The C-H stretches are shifted to the red compared to those in isolated C_2H_6 (2896 and 2954 cm^{-1} for CH_3 symmetric stretches and 2969 and 2985 cm^{-1} for antisymmetric stretches).[53] The red shift of the lowest-frequency C-H stretch is approximately 200 cm^{-1}, but different clusters show different patterns in their vibrational spectra. The peaks in the antisymmetric stretch region (~2950-3000 cm^{-1}) are weak or not observed.

To determine which isomers are produced in the experiment, vibrational spectra of likely isomers are compared to the experimental spectra. The calculations of the entrance channel

complexes between $Al_xO_y^+$ and C_2H_6 start with the calculated structures of $Al_xO_y^+$ reported by Khanna's group[50] and add ethane at various possible sites. The geometry is then optimized and vibrational frequencies and absorption intensities are calculated. As expected, the ethane binds to Al, which withdraws electron density from the proximal C-H bonds, weakening them and resulting in a red shift in the proximal C-H stretch. The interaction between Al and ethane also polarizes the C-H bond, which enhances IR absorption intensity. These effects are characteristic of hydrocarbons interacting with metal cations.[54] The bond dissociation energies (BDEs) and relative energies (E_{rel}) of calculated isomers are shown in Table 2. The BDEs all depend strongly on the composition of the $Al_xO_y^+$ core. The potential energy surfaces for the $Al_xO_y^+ + C_2H_6$ reaction, structures of reaction intermediates and their vibrational spectra will be discussed individually in detail, classified into two groups by their spin multiplicity: singlets ($Al_3O_2^+$ and $Al_3O_4^+$) and then doublets (Al_2O^+ and $Al_4O_7^+$).

Table 2. Calculated bond dissociation energies (BDEs) for loss of C_2H_6, C_2H_5 and C_2H_4, and relative energies (E_{rel}) of possible isomers for the reaction products of several $Al_xO_y^+(C_2H_6)_n(N_2)_k$ at the B3LYP/TZVP level of theory.

Species	Isomer	BDE		E_{rel}	
		kJ/mol	cm^{-1}	kJ/mol	cm^{-1}
$[Al_2OC_2H_6]^+$					
$Al_2O^+ + C_2H_6$				12.6	1053
Al_2O^+–(C_2H_6)	I	12.6	1053	0.0	0
	II	12.2	1020	0.4	33
	III	10.0	836	2.6	217
Al_2OH^+–(C_2H_5)	I	112.8	9429	28.5	2382
	II	112.5	9404	28.8	2407
$Al_2OH_2^+$–(C_2H_4)	I	99.1	8284	55.1	4606
$[Al_3O_2C_2H_6]^+$					
$Al_3O_2^+ + C_2H_6$				42.7	3570
$Al_3O_2^+$–(C_2H_6)	I	40.0	3344	2.7	226
$Al_3O_2H^+$–(C_2H_5)	I	298.3	24936	0.0	0

	II	297.1	24836	1.2	100
$Al_3O_2H_2^+$–(C_2H_4)	I	23.6	1973	222.0	18558
$[Al_3O_2C_2H_6N_2]^+$					
$Al_3O_2^+$(C_2H_6)–(N_2)	I	22.7	1898	0.0	0
$[Al_3O_4C_2H_6]^+$					
$Al_3O_4^+$ + C_2H_6				331.8	27736
$Al_3O_4^+$–(C_2H_6)	I	108.8	9095	223.0	18641
$Al_3O_4H^+$–(C_2H_5)	I	306.3	25605	0.0	0
$Al_3O_4H_2^+$–(C_2H_4)	I	90.6	7574	35.9	3001
$[Al_3O_4C_4H_{12}]^+$					
$Al_3O_4^+$(C_2H_6)–(C_2H_6)	I	91.0	7607	0.0	0
$[Al_3O_4C_6H_{18}]^+$					
$Al_3O_4^+$(C_2H_6)$_2$–(C_2H_6)	I	76.2	6370	124.0	10366
	II	76.0	6353	124.2	10382
	III	5.7	476	194.5	16259
	IV	3.1	259	197.1	16476
	V	3.0	251	197.2	16485
$Al_3O_4H^+$(C_2H_6)(C_2H_5)–(C_2H_6)	I	16.1	1346	0.0	0
$Al_3O_4H_2^+$(C_2H_6)(C_2H_4)–					
(C_2H_6)	I	5.8	485	82.3	6880
$[Al_4O_7C_2H_6]^+$					
$Al_4O_7^+$ + C_2H_6				335.5	28046
$Al_4O_7^+$–(C_2H_6)	I	94.6	7908	240.9	20138
	II	91.8	7674	243.7	20372
	III	73.2	6119	262.3	21926
	IV	72.8	6086	262.7	21960
	V	5.0	418	330.5	27628
	VI	4.9	410	330.6	27636
$Al_4O_7H^+$–(C_2H_5)	I	143.2	11971	270.3	22595
	II	41.0	3427	372.5	31138
$Al_4O_7H_2^+$–(C_2H_4)	I	141.7	11845	0.0	0

II	20.3	1697	121.5	10157
III	20.0	1672	121.7	10173

III. B. 2. $Al_3O_2^+(C_2H_6)$ and $Al_3O_2^+(C_2H_6)(N_2)$

We measured vibrational spectra of stoichiometric $[Al_3O_2C_2H_6]^+$ and $[Al_3O_2C_2H_6N_2]^+$ in the C-H stretching region (2600-3100 cm^{-1}) by infrared photodissociation spectroscopy. As will be discussed later, $[Al_3O_2C_2H_6]^+$ and $[Al_3O_2C_2H_6N_2]^+$ are determined to be $Al_3O_2^+(C_2H_6)$ and $Al_3O_2^+(C_2H_6)(N_2)$, respectively. To find the appropriate method to simulate the spectra, we compared the experimental spectra to simulations from scaled harmonic B3LYP/TZVP calculations and local mode Hamiltonian (LMH) calculations[49] at the B3LYP/6-311+G(d,p), B3LYP+D3/6-311+G(d,p) and ωB97X-D/6-311+G(d,p) levels. The LMH method was developed with these functionals and the 6-311+G(d,p) basis set, based on calculations on alkyl benzenes.[48,49] It includes the effect of C-H stretching anharmonicity and contributions to the spectrum from C-H bend overtones. This allows us to carry out an anharmonic simulation of the spectrum with computational effort only slightly larger than for a harmonic calculation.

As shown in Fig. S10, simulations using three methods (scaled harmonic B3LYP/TZVP and LMH using B3LYP/6-311+G(d,p) and B3LYP+D3/6-311+G(d,p)) are very similar and are an excellent match to the experiment spectra, while LMH ωB97X-D/6-311+G(d,p) is clearly inferior. The LMH results at the B3LYP and B3LYP+D3 levels are nearly indistinguishable. They do a better job of reproducing the smaller peaks at 2830 and 3005 cm^{-1} in the $Al_3O_2^+(C_2H_6)(N_2)$ spectrum than the scaled harmonic calculation. Similar results are obtained for other clusters in this work. Therefore, we will simulate spectra using LMH B3LYP/6-311+G(d,p) for all the isomers that contain -CH_3 units and will use scaled simulated spectra from B3LYP/TZVP for the rest, as the LMH code requires that the molecule contain at least one -CH_3 unit.[49] The reported geometries, energies and charges are at the B3LYP/TZVP level of theory to be consistent with previous studies, which have shown that this level of theory is reliable for aluminum oxide cluster ions and their interactions with hydrocarbons.[7,15,36]

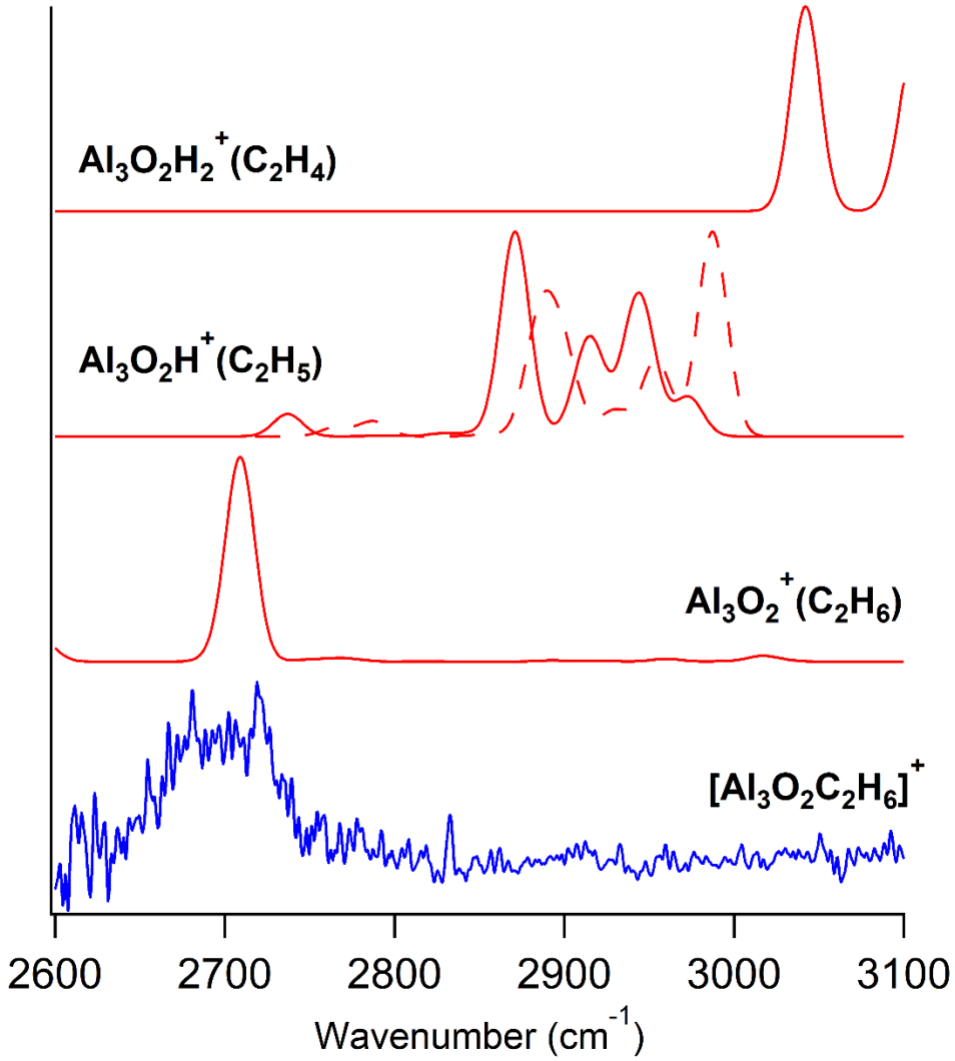

Figure 3. Vibrational spectrum of stoichiometric $[Al_3O_2C_2H_6]^+$ in the C-H stretching region (2600-3100 cm^{-1}) (blue). The simulated spectra of the low-lying isomers (red) are at the local-mode Hamiltonian, B3LYP/6-311++G(d,p) level, except for $Al_3O_2H_2^+(C_2H_4)$ which is at the scaled harmonic, B3LYP/TZVP level of theory.

$Al_3O_2^+$ is the most abundant small ion over a wide range of conditions. It reacts efficiently with ethane to form $[Al_3O_2C_2H_6]^+$. The spectrum (Fig. 3) consists of a broad, symmetric peak at 2702 cm^{-1}. In order to determine the structure of this ion, we calculate the vibrational spectrum of candidate structures and compare them to the experimental spectrum. The simulated spectra of $Al_3O_2H^+(C_2H_5)$ and $Al_3O_2H_2^+(C_2H_4)$ (structures in Fig. 4) are obviously not similar to the experiment. As will also be seen for other clusters, the C-H stretches of the $-C_2H_5$ group occur near

2870-2990 cm^{-1}, while those of the C_2H_4 group lie at and above ~3040 cm^{-1}. These are >150 cm^{-1} to the blue of the measured peaks. The simulated spectrum of $Al_3O_2^+(C_2H_6)$ is a good match to experiment. This is also consistent with the only photofragment observed being $Al_3O_2^+$ (loss of C_2H_6). Larger adducts, $Al_3O_2^+(C_2H_6)_n$ are not seen. The geometry of $Al_3O_2^+$ is calculated to be linear, in agreement with a previous study by Armstrong et al.[50]

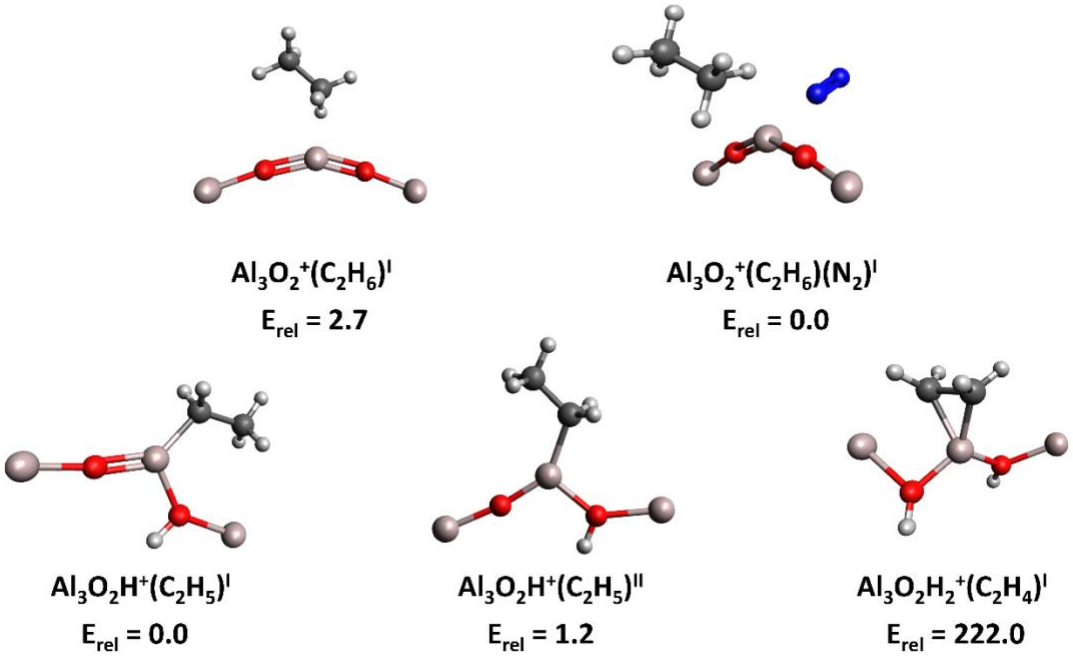

Figure 4. Optimized geometries of $[Al_3O_2C_2H_6]^+$ isomers and their relative energies (kJ/mol).

It transforms to a slightly bent structure when it forms an adduct with C_2H_6, as shown in Fig. 4. Initial structures with the C_2H_6 oriented side-on and end-on, and near the terminal or central Al all ended up with the same final geometry when optimized. In the optimized geometry, the C_2H_6 is bound to the central aluminum, which has the highest partial positive charge (+0.66 e^- while the other two Al are +0.38 e^-). Two hydrogens are coordinated to the metal (η^2 coordination), all of the heavy atoms are in the same plane, and $r_{Al\text{-}C}$ is 2.396 Å. The LMH calculation shows the major peak is at 2709 cm^{-1} and is due to the symmetric stretch of the C-H bonds proximal to the Al. This is in good agreement with the observed peak at 2702 cm^{-1}. Binding to the $Al_3O_2^+$ red shifts the lowest C-H stretching frequency from ν_5 = 2895.8 cm^{-1} in pure C_2H_6 to 2702 cm^{-1}. The calculations also predict that the proximal C-H bond lengths increase from 1.090 Å to 1.114 Å. This shows that $Al_3O_2^+$ weakens the C-H bonds, showing some potential for C-H bond activation.

However, these shifts are much smaller than is observed with many transition metals, and the calculations (Table 2 and Figure S8) reveal that abstraction of the H atom of C_2H_6 to form C_2H_5 or C_2H_4 is very endothermic. This was the reason that there was no product observed from $Al_3O_2^+$ C-H activation. Thus, it is not surprising that Shuman et al.[32] observe no reaction between $Al_3O_2^+$ and methane.

The other C-H stretches are much less intense. Those due to the proximal antisymmetric C-H stretches (with some contribution from bending overtones) are calculated to be at 2748, 2764 and 2776 cm^{-1}. Those due to the distal C-H bonds are predicted to be at 2960 cm^{-1} (symmetric stretch), and 3015 and 3017 cm^{-1} (antisymmetric stretch). They are not observed in the experimental spectrum. For the nitrogen-tagged complex $Al_3O_2^+(C_2H_6)(N_2)$, the experimental spectrum has an intense peak at 2740 cm^{-1}. This is 38 cm^{-1} smaller red shift than in the untagged complex. Tagged ions typically show smaller red shifts, as the tag slightly reduces the charge on the ion. This peak is calculated to lie at 2744 cm^{-1} and is due to the proximal symmetric stretch, with the amplitude weighted towards the C-H bond nearest the N_2. In addition, there are now two smaller peaks clearly observed in the experimental spectrum, at 2830 and 3005 cm^{-1}. These are assigned to the proximal antisymmetric stretch (amplitude primarily of the C-H bond pointing away from the N_2) calculated at 2839 cm^{-1} and to the distal antisymmetric stretches calculated at 3011 and 3013 cm^{-1}.

III. B. 3. $Al_3O_4^+(C_2H_6)_n$

$Al_3O_4^+$ has been identified as a stable core structure for the $Al_3O_{4+2n}^+$ series.[30] In previous work, the geometry of $Al_3O_4^+$ was assigned by comparing experimental vibrational spectra with the calculation of possible isomers. They discovered that $Al_3O_4^+$ possesses a cage-like structure with C_{3v} symmetry where Al and O alternate to form a six-membered ring and the last O binds on the center-top of the ring.[29,30,55] In this work, the $Al_3O_4^+$ system was also studied. We measured the vibrational spectrum of stoichiometric $[Al_3O_4C_6H_{18}]^+$. The constitutional isomers of stoichiometric $[Al_3O_4C_6H_{18}]^+$ can be $Al_3O_4^+(C_2H_6)_3$, $Al_3O_4H^+(C_2H_6)_2(C_2H_5)$, $Al_3O_4H_2^+(C_2H_6)_2(C_2H_4)$; the ions $Al_3O_6^+(C_2H_6)(C_2H_4)$, $Al_3O_8^+(C_2H_2)$ and $Al_4O_6H^+(C_2H_6)$ also have the same nominal mass. In order to distinguish these clusters, further study is required. The mass spectrum and laser on-laser off difference mass spectrum of $[Al_3O_4C_6H_{18}]^+$ in Fig. S11 shows loss of one and two ethane, eliminating the possibility of additional isomers that do not contain

intact C_2H_6. Therefore, the possible isomers ought to be a product(s) from the reaction of $Al_3O_4^+$ with C_2H_6 which are $Al_3O_4^+(C_2H_6)_3$, $Al_3O_4H^+(C_2H_5)(C_2H_6)_2$, $Al_3O_4H_2^+(C_2H_4)(C_2H_6)_2$, or the isobaric $Al_3O_6^+(C_2H_6)(C_2H_4)$ and $Al_4O_6H^+(C_2H_6)$.

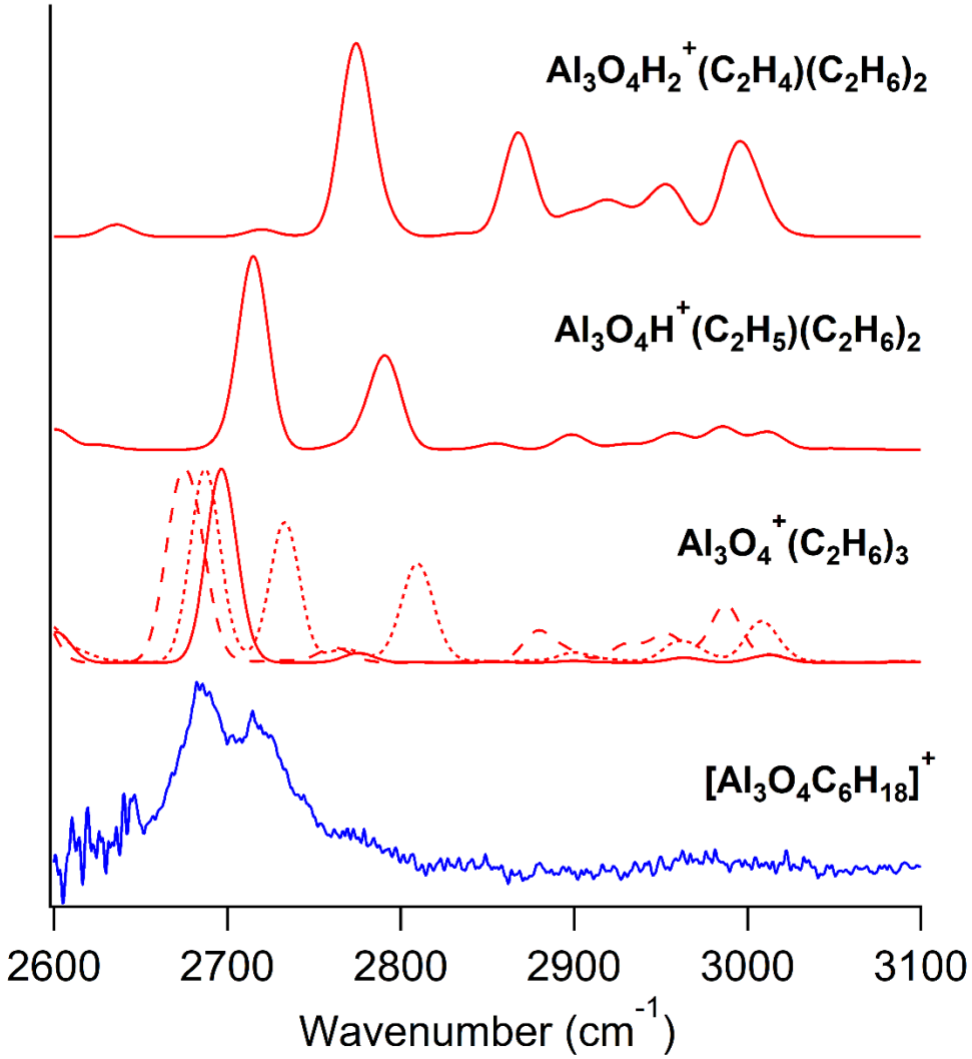

Figure 5. Vibrational spectrum of stoichiometric $[Al_3O_4C_6H_{18}]^+$ in the C-H stretching region (2600-3100 cm^{-1}) (blue). The simulated spectra of the low-lying isomers (red) are at the local-mode Hamiltonian, B3LYP/6-311++G(d,p) level of theory. See text for details on isomers.

The experimental spectrum of stoichiometric $[Al_3O_4C_6H_{18}]^+$ is shown in Fig. 5, along with calculated spectra of low-lying isomers. Calculated spectra of isomers of isobaric $Al_3O_6^+(C_2H_6)(C_2H_4)$ and $Al_4O_6H^+(C_2H_6)$ are shown in Fig. S12. The experimental spectrum consists of an intense doublet at 2685 and 2718 cm^{-1} (33 cm^{-1} peak separation) and a weak, broad

shoulder near 2780 cm^{-1}. The $Al_3O_6^+(C_2H_6)(C_2H_4)$ and $Al_4O_6H^+(C_2H_6)$ ions likely do not contribute to the observed spectrum. The calculated spectrum of $Al_3O_6^+(C_2H_6)(C_2H_4)^I$, is not a good match, as the most intense peak is at 2653 cm^{-1}, well to the red of the doublet in the experimental spectrum. Although the calculated spectrum of the $Al_4O_6H^+(C_2H_6)$ isomer shows a peak at 2709 cm^{-1} that matches well with the experimental peak at 2718 cm^{-1}, the formation of $Al_4O_6H^+(C_2H_6)$ is unfavorable for the reaction of $Al_xO_y^+$ with C_2H_6 because it needs to form a neutral radical product ($C_2H_5\cdot$) which is very unstable.

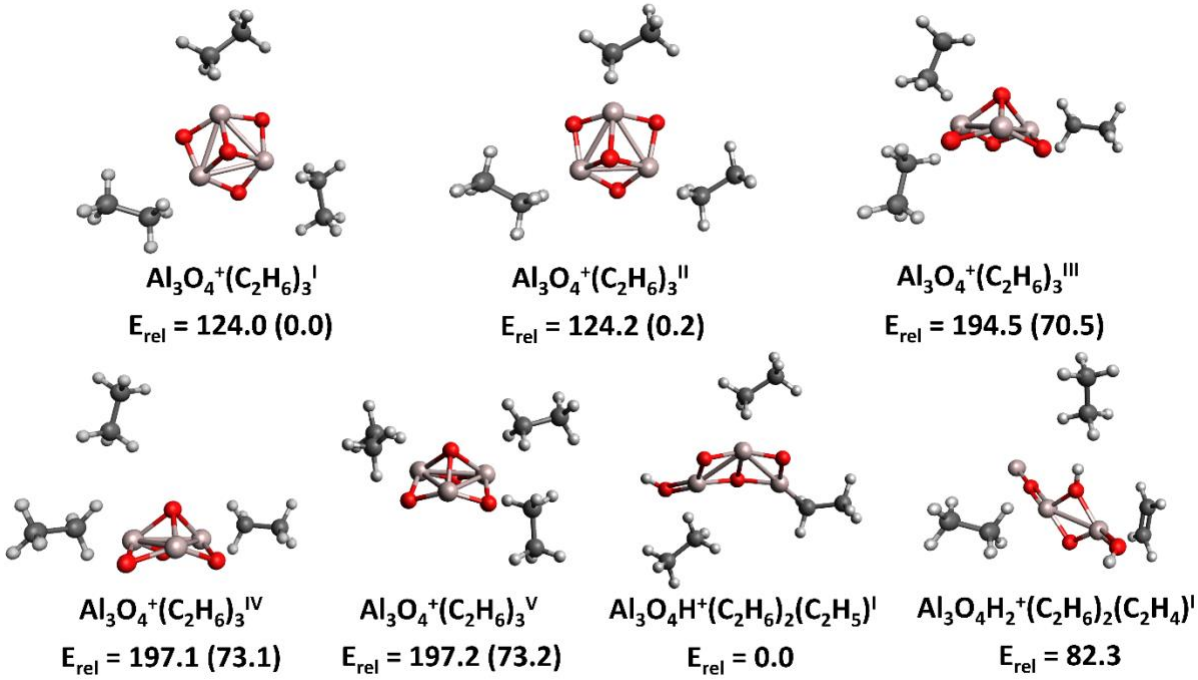

Figure 6. Optimized geometries of $[Al_3O_4C_6H_{18}]^+$ isomers and their relative energies (kJ/mol). The number in parentheses shows the relative energies of stereoisomers.

The entire observed spectrum can be assigned to isomers of the $Al_3O_4^+(C_2H_6)_3$ entrance channel complex and C-H activation intermediates. The lowest-energy isomer of the entrance channel complex, $Al_3O_4^+(C_2H_6)_3^I$ (spectrum in solid line, Fig. 5), has C_3 symmetry (structure in Fig. 6). Each ethane binds to a different aluminum atom using η^2 hydrogen coordination. The proximal C-H bonds lengthen to 1.115-1.119 Å compared to isolated ethane (1.092 Å). As a result, the intense C-H symmetric stretch red shifts significantly and is calculated to be at 2697 cm^{-1}. This partially corresponds to the observed spectrum, but would not lead to a doublet. Note that $Al_3O_4^+(C_2H_6)^I$ is predicted to show an even larger red shift, to $\nu_{C\text{-}H}$ = 2663 cm^{-1} and distortion, $r_{C\text{-}}$

$_H$ = 1.117 to 1.122 Å. Fewer ligands in the cluster lead to stronger metal-ligand interactions. This results in a larger red shift (and a longer C-H bond length) than in $Al_3O_4^+(C_2H_6)_3^I$. Compared to $Al_3O_2^+(C_2H_6)$, the $Al_3O_4^+(C_2H_6)^I$ also has a larger red shift. This is consistent with $Al_3O_4^+$ being more reactive towards ethane than $Al_3O_2^+$, as shown by the calculated energies in Table 1.

There is one other low-energy isomer of $Al_3O_4^+(C_2H_6)_3$ and three at slightly higher energy (Fig. 6). The $Al_3O_4^+(C_2H_6)_3^{II}$ isomer differs from $Al_3O_4^+(C_2H_6)_3^I$ only by a 120° rotation of one ethane. As a result, the C-H bond lengths are unchanged and the calculated spectrum is nearly identical (1 cm^{-1} shift) and is not shown. In the higher energy $Al_3O_4^+(C_2H_6)_3^{IV}$ isomer, one ethane is in the second shell. Its calculated spectrum (dashed line, Fig. 5), contains a strong peak at 2675 cm^{-1} assigned to the proximal C-H symmetric stretches of the two inner-sphere ethanes that bind directly to different aluminum atoms in the cluster. This is a larger red shift than in the $Al_3O_4^+(C_2H_6)_3^I$ isomer as fewer ethanes are bound to the $Al_3O_4^+$ core, and is somewhat more red shifted than is experimentally observed. There is also a weaker peak at 2880 cm^{-1} assigned to the corresponding vibration of the weakly bound outer-sphere ethane. This peak has a much smaller red shift than other proximal C-H symmetric stretches because the ligand is not directly correlated to an aluminum atom in the cluster, leading to a weaker interaction between an aluminum atom and a ligand. It is also less intense, as the C-H bond is not polarized by an adjacent cation. The C-H bond lengths are predicted to be 1.114-1.121 Å for proximal inner-sphere ethane and 1.094 Å for proximal outer-sphere ethane. There is no clear indication that $Al_3O_4^+(C_2H_6)_3^{IV}$ contributes to the experimental spectrum.

The calculated spectra of $Al_3O_4^+(C_2H_6)_3^{III}$ and $Al_3O_4^+(C_2H_6)_3^V$ (dotted line, Fig. 5) are nearly identical and are a poor match to the experiment. In these isomers, two ethanes bind to the same aluminum, while the third binds to another aluminum (Fig. 6). As a result, the ethanes are not equivalent, leading to the three intense peaks at 2687, 2733, and 2810 cm^{-1}.

We also calculated the spectra of two C-H activation intermediates: $Al_3O_4H^+(C_2H_5)(C_2H_6)_2$ and $Al_3O_4H_2^+(C_2H_4)(C_2H_6)_2$ (Fig. 5). $Al_3O_4H_2^+(C_2H_4)(C_2H_6)_2$ clearly does not match the observed spectrum. The lowest-lying isomer is $Al_3O_4H^+(C_2H_5)(C_2H_6)_2$, in which the $Al_3O_4^+$ core structure changes from a cage-like structure to a planar (C_s) structure (Fig. 6). The hydrogen atom attaches to the non-bridging oxygen and C_2H_5 binds to a corner aluminum atom. Its calculated spectrum shows an intense peak at 2718 cm^{-1}, matching the observed peak at 2718 cm^{-1}. The simulation also predicts a less intense peak at 2791 cm^{-1}, which may be responsible for the weak and partially

resolved peak observed near 2780 cm^{-1}. Therefore, this C-H activation intermediate, $Al_3O_4H^+(C_2H_5)(C_2H_6)_2$, is likely to contribute to the experimental spectrum.

In summary, none of the calculated isomers reproduces the entire experimental spectrum we observed individually. The combination of calculated spectra of the entrance channel complexes $Al_3O_4^+(C_2H_6)_3^I$/$Al_3O_4^+(C_2H_6)_3^{II}$ and C-H activation intermediate $Al_3O_4H^+(C_2H_5)(C_2H_6)_2$ captures the entire observed spectrum very well with an intense doublet separated by 21 cm^{-1}.

The calculated potential energy surface of the reaction between $Al_3O_4^+$ and one C_2H_6 is shown in Fig. S9. Even though the reactions to form ethyl radical and ethene are exothermic by 26 and 219 kJ/mol, respectively, there is a submerged barrier to the first C-H activation that is only 13 kJ/mol below the reactant energy. As a result, the entrance channel complex, which is bound by 109 kJ/mol, is sufficiently long-lived (~2 ms, based on RRKM calculations)[56] that it is efficiently stabilized by collisions with the helium buffer gas. Thus, some reactants are trapped at the entrance channel complex, $Al_3O_4^+(C_2H_6)_3^{I/II}$, while some proceed to form the very stable C-H activation intermediate $Al_3O_4H^+(C_2H_5)$, which is longer-lived (~60 ms RRKM lifetime) and is stabilized by collisions so it does not undergo a second C-H activation or form $Al_3O_4H^+ + C_2H_5$. Shuman et al.[32] observed similar results for the reaction of $Al_3O_4^+$ with methane: adducts are the only observed products, and are produced at ~50% of the collision rate. This is a far higher rate than they measured for $Al_3O_2^+$ and Al_2O^+, which is consistent with the $Al_xO_y^+$-C_2H_6 binding energies (Table 2) which are in the order $Al_3O_4^+ > Al_3O_2^+ > Al_2O^+$.

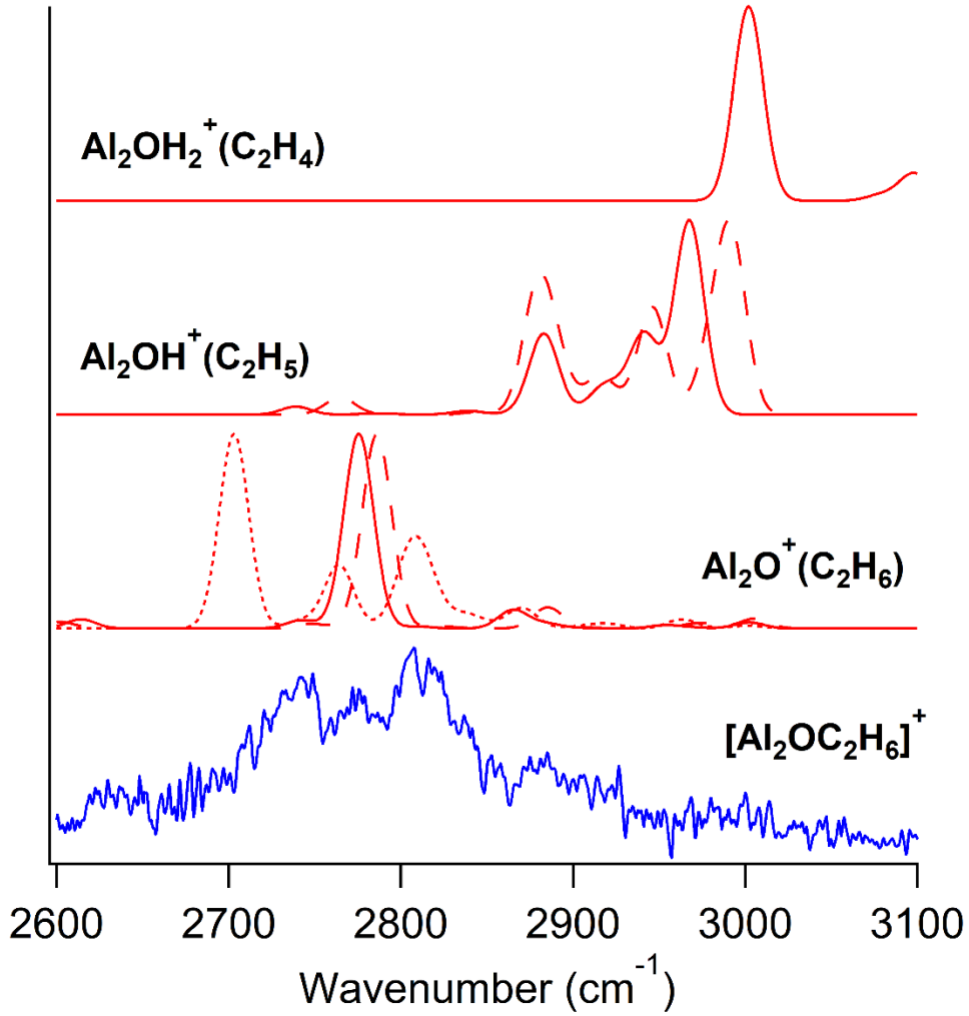

Figure 7. Vibrational spectrum of stoichiometric $[Al_2OC_2H_6]^+$ in the C-H stretching region (2600-3100 cm^{-1}) (blue). The simulated spectra of the low-lying isomers (red) are at the local-mode Hamiltonian, B3LYP/6-311++G(d,p) level, except for $Al_2OH_2^+(C_2H_4)$ which is at the scaled harmonic, B3LYP/TZVP level of theory. See text for details on the isomers.

III. B. 4. $Al_2O^+(C_2H_6)$

Al_2O^+ is the smallest aluminum oxide cluster ion with an even number of aluminum atoms. Its geometry is calculated to be linear Al-O-Al, in agreement with calculations by Armstrong et al.[50] The experimental spectrum of stoichiometric $[Al_2OC_2H_6]^+$ is shown in Fig. 7. The spectrum consists of an intense triplet (at 2740, 2774 and 2812 cm^{-1}) and three less intense peaks (at 2630, 2882 and ~3000 cm^{-1}). The calculated spectra of the C-H activation intermediates $Al_2OH^+(C_2H_5)^I$,

$Al_2OH^+(C_2H_5)^{II}$, and $Al_2OH_2^+(C_2H_4)^I$ (structures in Fig. 8) are well to the blue of the observed peaks and they are not likely to contribute to the observed spectrum.

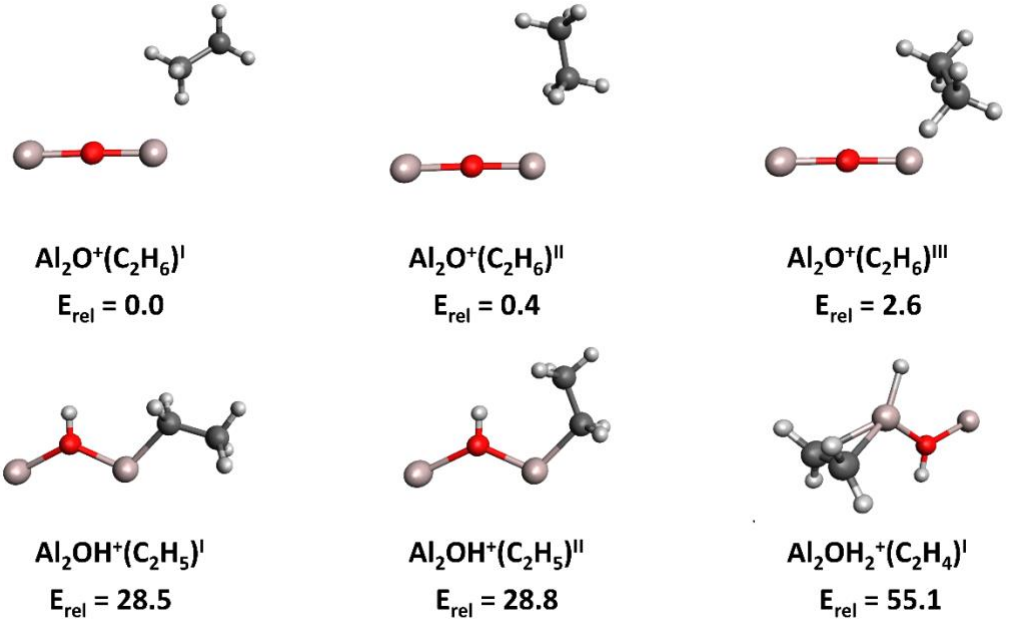

Figure 8. Optimized geometries of $[Al_2OC_2H_6]^+$ isomers and their relative energies (kJ/mol).

The calculations predict that the lowest-energy isomer is $Al_2O^+(C_2H_6)^I$ (solid line, Fig. 7), in which an ethane binds end-on to an aluminum atom with η^2 hydrogen coordination (Fig. 8). The proximal C-H bonds elongate to 1.105 Å, compared 1.092 Å in isolated ethane. As a result, the C-H symmetric stretch is predicted to red shift to 2776 cm^{-1}. Minor peaks are also predicted to be at 2614 and 2866 cm^{-1} which come from bending overtones/combination bands. The calculated spectrum partly reproduces the experiment spectrum, with the peak at 2776 cm^{-1} matching the middle intense peak of the experiment. There are also two other low-lying isomers of $Al_2O^+(C_2H_6)$. The $Al_2O^+(C_2H_6)^{II}$ and $Al_2O^+(C_2H_6)^{III}$ isomers (Fig. 8) are calculated to be only 33 and 217 cm^{-1} (Table 2) less stable than the lowest energy isomer. $Al_2O^+(C_2H_6)^{II}$ (dashed line, Fig. 7) has similar geometry to $Al_2O^+(C_2H_6)^I$, with different ethane orientation. The calculated spectrum has very similar pattern to that of $Al_2O^+(C_2H_6)^I$ with an approximately 10 cm^{-1} shift to the blue. The most intense peak is calculated to be at 2786 cm^{-1} and is also in good agreement with the middle intense peak of the obtained vibrational spectrum. In the calculated $Al_2O^+(C_2H_6)^{III}$ isomer (dotted line, Fig. 7), the ethane binds side-on, with one H atom from each carbon binding to an aluminum atom.

The proximal C-H bonds are not equivalent, leading to intense peaks at 2703 and 2808 cm^{-1} assigned to the proximal C-H stretches, as well as a peak at 2764 cm^{-1} assigned to a bending overtone. There are also minor peaks at 2870 and 2963 cm^{-1} due to bending overtone/combination band and distal C-H symmetric stretch respectively. The calculated peak positions of $Al_2O^+(C_2H_6)^{III}$ match the triplet in the observed spectrum, although the intensities do not. In addition, the simulation does not have a peak near 2630 cm^{-1}.

No single simulated spectrum is able to reproduce the entire observed spectrum. However, considering the small energy differences between the $Al_2O^+(C_2H_6)$ isomers, it is likely that the experimental spectrum is due to more than one isomer. Figure S13 shows the combination of the simulated spectra of the side-on isomer, $Al_2O^+(C_2H_6)^{III}$, and one of the end-on isomers, $Al_2O^+(C_2H_6)^{I}$. Since the end-on isomers (I and II) have very similar spectra, we only include the simulated spectrum of the lowest-lying isomer. With a 3:7 ratio of $Al_2O^+(C_2H_6)^{I}$ to $Al_2O^+(C_2H_6)^{III}$, the simulated spectrum provides a good match to the experiment. Competing contributions of side-on and end-on isomers have been observed by our group for complexes of V^+, Al^+ and Al_2^+ with ethane.[54,57] Therefore, the experimental spectrum can be assigned to be the adduct between Al_2O^+ and C_2H_6. This is also consistent with our observation that the only photofragment observed is loss of C_2H_6.

As discussed in Section III A, Al_2O^+ is a doublet and thus would be expected to be reactive toward ethane. However, the cluster is oxygen deficient, which should make it less reactive than oxygen-rich species. Reactivity is enhanced when the unpaired electron is localized on a (non-bridging) O atom. In Al_2O^+, the oxygen atom is bridging and the unpaired electron is shared between the Al atoms. Oxygen atoms can also facilitate C-H bond activation by forming an O-H bond, but this is less favorable for oxygen-deficient clusters, as it disrupts strong Al-O-Al bonds. As shown in Fig. S14, the calculated potential energy surface demonstrates that C-H activation is endothermic and has large barriers (≥130 kJ/mol). As a result, we do not observe any C-H bond activation intermediates. This agrees with the results of Shuman et al.,[32] who found that Al_2O^+ does not react with methane or ethane (upper limit of 1% of the collision rate).

$Al_2O_2^+$ is the smallest cluster which has been found to activate methane.[31] Unfortunately, we are unable to form sufficient amounts of $Al_2O_2^+$ for a spectroscopic study due to its high reactivity. Shuman et al.[32] have studied the temperature-dependent kinetics of the reaction of

$Al_2O_2^+$ with C_2H_6. The reaction occurs approximately at the collision rate and there are three product channels: 1) association: $Al_2O_2^+(C_2H_6)$ adduct or other isomers, ~50% branching at 300 K, decreasing sharply with increasing temperature; 2) $Al_2O_2H_2^+ + C_2H_4$, ~50% branching at 300 K, decreasing slowly with increasing temperature; 3) $Al_2O_2H^+ + C_2H_5$, ~2% branching at 300 K, increasing sharply with increasing temperature. We calculated the potential energy surface for the $Al_2O_2^+ + C_2H_6$ reaction at the B3LYP/TZVP level of theory, Figure S6 and Table 1. The initially-formed entrance channel complex $Al_2O_2^+(C_2H_6)$ can be stabilized by collisions (leading to an association product), or can surmount TS1 (which lies just below the reactants) to form a hydrogen abstraction intermediate $Al_2O_2H^+$-C_2H_5. This can then fall apart to form $Al_2O_2H^+ + C_2H_5$ or undergo a second hydrogen abstraction via TS2 to form the $Al_2O_2H_2^+(C_2H_4)$ exit channel complex, which then produces $Al_2O_2H_2^+ + C_2H_4$. The loose dissociation to C_2H_5 is entropically favored and energetically dis-favored over the tight TS2 isomerization. As a result, formation of C_2H_4 dominates at low temperature, but the C_2H_5 channel becomes increasingly important at higher temperatures, in accord with experiment. Higher temperatures would also disfavor collisional stabilization of the reaction intermediates (observed as association products).

III. B. 5. $Al_4O_7^+(C_2H_6)$

In their study of the vibrational spectra of $Al_xO_y^+$, Kiawi et al.[30] observed that the very oxygen-rich species in the $Al_4O_{7+2n}^+$ series (where n = 1, 2) lose molecular oxygen down to $Al_4O_7^+$ following IRMPD, while there is no formation of $Al_4O_5^+$, revealing that $Al_4O_7^+$ is the stable core structure for the $Al_4O_{7+2n}^+$ series. Even $Al_4O_7^+$ is considered an oxygen-rich cluster compared to its normal formula found in nature (Al_2O_3) and is calculated to have the structure shown in Fig. 9, with C_s symmetry and an O-O bond. Our calculations predict that the unpaired electron is shared between these two O atoms and that $r_{O\text{-}O}$ = 1.371 Å. Normally, in addition to molecular O_2, there are three possible types of oxygen active unit: O_2^-(superoxide), O_2^{2-}(peroxide), and O^- (oxygen-centered radical).[58] The calculated O-O bond lengths in these species are 1.208 (O_2), 1.354 (O_2^-)and 1.459 Å (O_2^{2-}, in H_2O_2). Based on the calculated spin distribution, O-O bond length and aluminum oxidation state, the O-O moiety in $Al_4O_7^+$ is a superoxide. This result is consistent with a previous study from Perera et al.[59] where $TaO_x^{0/+}$ (x = 3-6), were calculated to often have superoxide structures.

The experimental vibrational spectrum of stoichiometric $[Al_4O_7C_2H_6]^+$ shows an intense broad peak at 2704 cm^{-1} with FWHM ~95 cm^{-1} (Fig. 10). Based on the mass of the selected peak, there are several possible isomers including $Al_4O_7^+(C_2H_6)$, $Al_4O_7H^+(C_2H_5)$, and $Al_4O_7H_2^+(C_2H_4)$ as shown in Fig. 9. The lowest-lying isomer is $Al_4O_7H_2^+(C_2H_4)^I$. In this structure, each O atom on the triangular bidentate site abstracts a hydrogen, forming ethene. The ethene then migrates to the opposite site of the cluster, binding to an Al atom. Other low-lying $Al_4O_7H_2^+(C_2H_4)$ stereoisomers, $Al_4O_7H_2^+(C_2H_4)^{II}$ and $Al_4O_7H_2^+(C_2H_4)^{III}$, have similar structures but with the ethene bound to different aluminum atoms, leading to similar calculated spectra. The calculated spectrum of $Al_4O_7H_2^+(C_2H_4)^I$ (Fig. 10) only has C-H stretches above 3000 cm^{-1} and is unlikely to contribute to the observed spectrum. Next, we performed calculations for $Al_4O_7H^+(C_2H_5)$. Their optimized geometries (Fig. 9) are analogous to those of $Al_4O_7H_2^+(C_2H_4)$ where rather than losing two H atoms, the ethane loses one H atom to an O atom on the triangular bidentate site and the remaining ethyl radical binds to an aluminum atom. They are at higher energy and their calculated spectra (Fig. 10) are also inconsistent with the observed spectrum. These results are consistent with the laser on – laser off difference spectrum, in which only the loss of C_2H_6 is observed. Hence, we performed calculations on $Al_4O_7^+(C_2H_6)$.

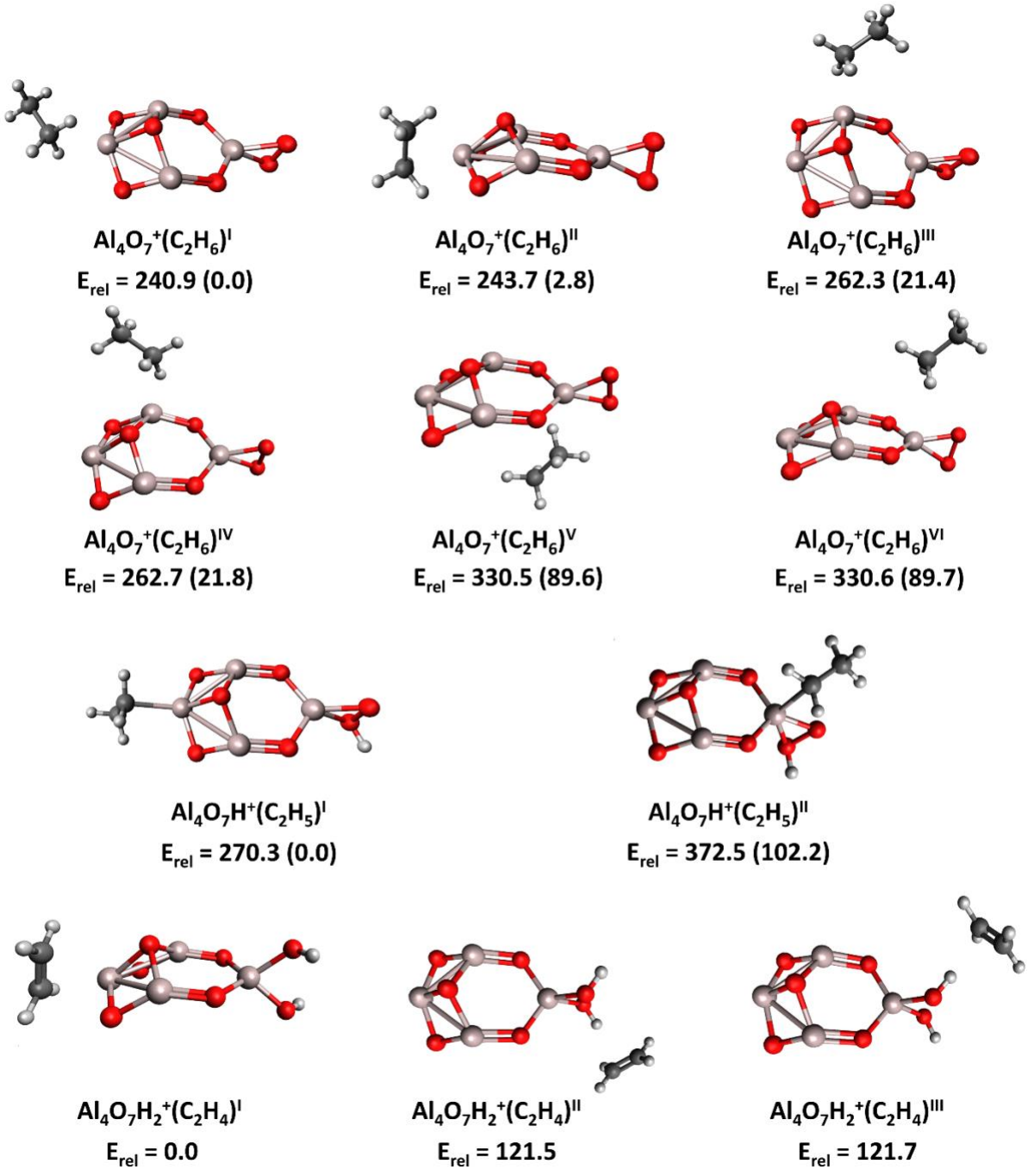

Figure 9. Optimized geometries of $[Al_4O_7C_2H_6]^+$ isomers and their relative energies (kJ/mol). The number in parentheses shows the relative energies of stereoisomers.

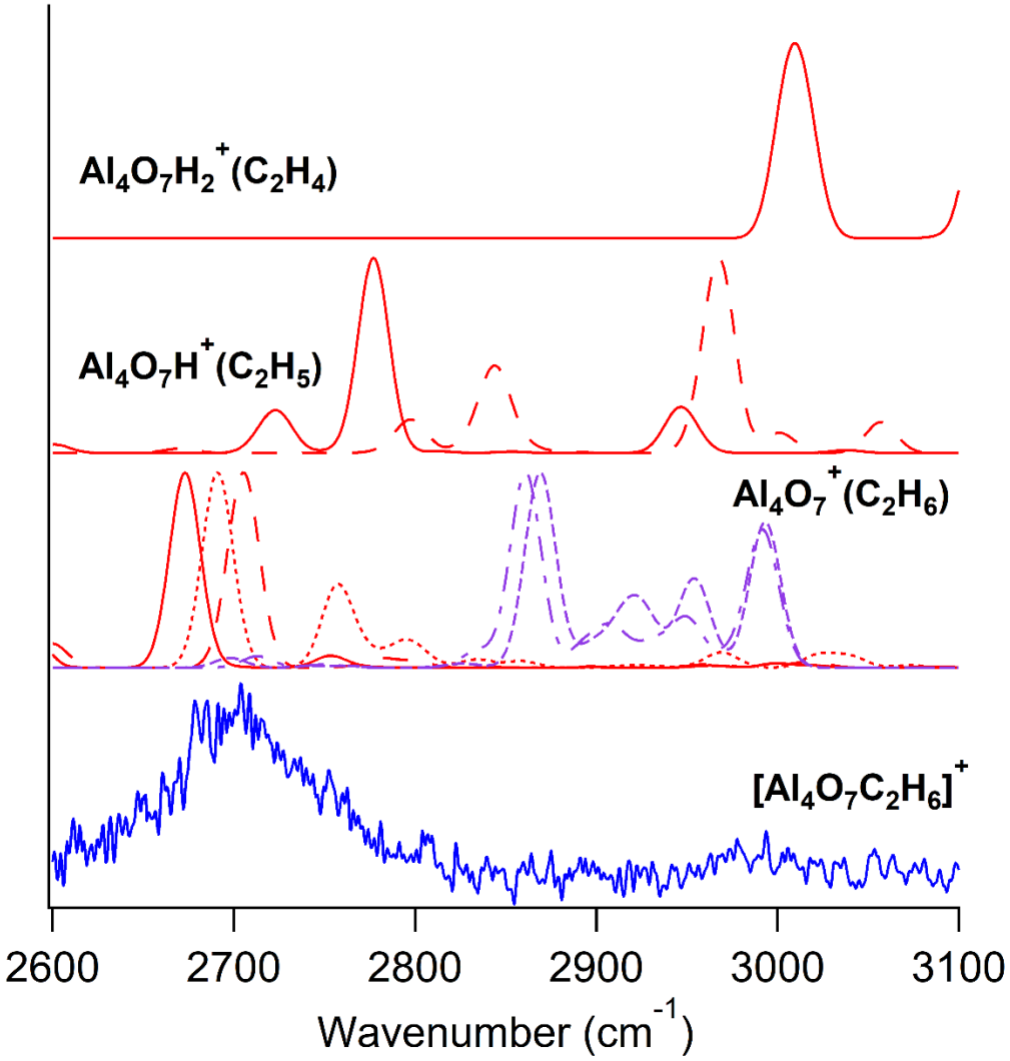

Figure 10. Vibrational spectrum of stoichiometric $[Al_4O_7C_2H_6]^+$ in the C-H stretching region (2600-3100 cm^{-1}) (blue). The simulated spectra of low-lying isomers (red, purple) are at the local-mode Hamiltonian, B3LYP/6-311++G(d,p) level, except for $Al_4O_7H_2^+(C_2H_4)$ which is at the scaled harmonic, B3LYP/TZVP level of theory. See text for details on isomers.

There are numerous $Al_4O_7^+(C_2H_6)$ stereoisomers with the same $Al_4O_7^+$ core and different positions and orientations of the ethane (Fig. 9). The structure of $Al_4O_7^+$ can be viewed as being comprised of a nearly planar eight-member Al_4O_4 ring with an additional O inside the ring, and a superoxide group attached to the outside of the ring. The lowest-lying isomer is $Al_4O_7^+(C_2H_6)^I$ in which the ethane binds opposite the superoxide. As shown in Fig. 10 (solid red line), the calculated spectrum of $Al_4O_7^+(C_2H_6)^I$ consists of an intense peak at 2673 cm^{-1}, which is slightly to the red of

the observed peak at 2704 cm^{-1}. This peak is due to the proximal C – H symmetric stretch of ethane bound to an aluminum atom with end-on η^2 coordination. In the second lowest-lying isomer, $Al_4O_7^+(C_2H_6)^{II}$ (dotted red line, Fig. 10), the ethane binds to the same aluminum atom, but side-on, so one hydrogen on each carbon interacts strongly with the metal. This leads to an intense peak at 2691 and a weaker peak at 2758 cm^{-1}, assigned to the proximal C – H stretch of the inequivalent H atoms in the ethane. The calculated spectrum also resembles the observed spectrum where both intense peaks sit in the region of the observed broad peak. This isomer is calculated to only be 234 cm^{-1} less stable than the lowest-lying $Al_4O_7^+(C_2H_6)$ isomer. There are two other low-lying isomers $Al_4O_7^+(C_2H_6)^{III}$ and $Al_4O_7^+(C_2H_6)^{IV}$ in which the ethane binds to the aluminum atom in the middle of the cluster using end-on η^2 coordination. They only differ in that ethane rotates 120˚ in $Al_4O_7^+(C_2H_6)^{IV}$ relative to $Al_4O_7^+(C_2H_6)^{III}$. Their simulated spectra are almost identical (< 1 cm^{-1} shift), so only the spectrum of $Al_4O_7^+(C_2H_6)^{III}$ is shown (dashed red line, Fig. 10). The simulated spectrum has an intense peak at 2705 cm^{-1}, from the proximal C – H symmetric stretch. It also provides a good match to the experimental result.

Furthermore, there are two other high-lying isomers: $Al_4O_7^+(C_2H_6)^{V}$ and $Al_4O_7^+(C_2H_6)^{VI}$ which have the proper orientation to be able to undergo C – H bond activation as the ethane is close to the superoxide ligand. They possess similar spectral patterns, two intense peaks and two other less intense peaks as shown in Fig. 10, in purple: dotted-dashed line for $Al_4O_7^+(C_2H_6)^{V}$ and short-dashed line for $Al_4O_7^+(C_2H_6)^{VI}$. Also, each of these isomers also has a nearly identical twin (the calculated spectrum shifts <1 cm^{-1} and energy difference <0.1 kJ/mol) in which the ethane rotates 120˚ and which is not shown here. These isomers are predicted to have much smaller red shifts in the proximal C-H stretches, so the calculated spectra are a poor match to the experimental spectrum, with intense peaks in regions where none are observed. Overall, from the calculated spectra of $Al_4O_7^+(C_2H_6)$ stereoisomers, there are four isomers ($Al_4O_7^+(C_2H_6)^{I/II/III/IV}$) that are likely to contribute to the vibrational spectrum. The breadth of the experimental peak makes it likely that more than one of these isomers contributes. There is no evidence for contributions from the higher-lying isomers $Al_4O_7^+(C_2H_6)^{V/VI}$.

The calculated potential energy surface for the reaction between $Al_4O_7^+$ and C_2H_6 is shown in Fig. S15. The first C – H bond activation is endothermic, but activation of the second C – H bond is extremely exothermic, and the $(HO)_2Al_4O_5^+(C_2H_4)$ isomers are very stable. We do not expect to observe C – H activation products as the barrier to the first C-H activation is substantial

(57 kJ/mol). In addition, in the entrance channel complexes $Al_4O_7^+(C_2H_6)^{V/VI}$ that have the proper orientation to be involved in C – H bond activation (blue) the ethane binds near the superoxide group, they lie well above the lowest-energy entrance channel complex $Al_4O_7^+(C_2H_6)^{I}$, in which the ethane is at the opposite end of the molecule. As noted above, in our experiment, near room temperature and with fairly high pressures of helium buffer gas, the lower-energy entrance channel complexes are stabilized and there is no indication of formation of the higher-energy entrance channel complexes or of C-H activation intermediates. However, at elevated temperatures, C-H activation is likely to occur.

The calculated binding energies of ethane to the $Al_xO_y^+$ clusters studied here vary greatly, ranging from very low (12.6 kJ/mol in Al_2O^+) to intermediate (40.0 kJ/mol in $Al_3O_2^+$) to high (94.6 and 108.8 kJ/mol in $Al_4O_7^+$ and $Al_3O_4^+$, respectively). We investigated the reasons for this using charge and molecular orbital analyses. As shown in Fig. S16, higher Mulliken charge on the Al to which the C_2H_6 will bind has an excellent linear correlation with larger binding energies, although the charges are in a fairly narrow range, from +0.656 in Al_2O^+ to 0.915 in $Al_3O_4^+$. This charge analysis is supported by a molecular orbital and formal charge picture. In Al_2O^+, the formal charge on each Al is 1.5+ and the HOMO is primarily an *s* orbital on the aluminums, which is repulsive towards ethane binding. In $Al_3O_2^+$, the terminal Al have a formal charge of 1+, while the central Al is 3+. The HOMO is an *s*-like orbital on the terminal aluminum atoms, and the ethane binds to the central Al. In $Al_4O_7^+$ and $Al_3O_4^+$, each aluminum has a 3+ formal charge. Molecular orbitals with significant charge density on 3+ Al atoms lie at energies at least 50 eV below the HOMO. The higher formal charge is reflected in a higher Mulliken charge and larger hydrocarbon binding energy.

IV. Summary and Conclusions

The reactions of $Al_xO_y^+$ with ethane were studied in a laser ablation, fast-flow reactor ion source. For a few species that are especially abundant, the reaction products were characterized using vibrational spectroscopy in the C-H stretching region, via photofragment spectroscopy. The experimental spectra of complexes of Al_2O^+, $Al_3O_2^+$, $Al_3O_4^+$ and $Al_4O_7^+$ with ethane, coupled with DFT calculations, reveal the structure and binding motifs of these ions. In each of these clusters, ethane remains intact and forms an adduct with the aluminum oxide cluster ion, resulting in the C – H bond weakening and a red shift of the proximal C – H symmetric stretch of ~200 cm^{-1}. Ethane

binds to an aluminum site in the cluster and there is a linear correlation between the $Al_xO_y^+$-C_2H_6 bond dissociation energy and the charge on the aluminum atom in $Al_xO_y^+$ to which the ethane will bind. Calculations of the potential energy surfaces for the reactions show that most have significant barriers to C-H activation and that hydrogen abstraction tends to occur at the oxygen site.

In the C-H stretching region, the simulated spectra of the reaction intermediates $Al_xO_y^+(C_2H_6)$, $Al_xO_y^+(C_2H_5)$ and $Al_xO_y^+(C_2H_4)$, are unique, so they can be readily distinguished. In addition, the spectra are sensitive to the coordination of the ethane. $Al_3O_2^+$ is calculated to have a large barrier to C-H activation. In accord, $Al_3O_2^+(C_2H_6)$ is observed to be an adduct between $Al_3O_2^+$ and end-on η^2 ethane. Meanwhile, $Al_3O_4^+$ is predicted to have a much more strongly-bound entrance channel complex and to only have a submerged barrier for C-H activation. At the relatively high pressures in our experiment, the $Al_3O_4^+(C_2H_6)$ entrance channel complex is collisionally stabilized and then readily proceeds to form an adduct with three ethanes. We also observe the C-H activation intermediate $Al_3O_4H^+(C_2H_5)$. Al_2O^+ is predicted to be the least reactive of the clusters studied. The spectrum of $Al_2O^+(C_2H_6)$ shows three distinct peaks, due to contributions from more than one isomer. The end-on and side-on isomers are predicted to be very close in energy, and they both contribute to the experimental spectrum. For $Al_4O_7^+(C_2H_6)$, the spectrum is notably broader than those of other clusters, indicating that multiple isomers contribute. The calculations reveal that the spectrum is due to isomers in which ethane is bound to aluminum atoms far from the superoxide site rather than to higher-lying isomers in which the ethane is adjacent to the superoxide and is positioned to undergo hydrogen abstraction.

As mentioned in the Introduction, the key reaction for enhancing jet engine performance is the formation of radical species because a hydrocarbon radical reacts much faster with oxygen than a non-activated hydrocarbon, which facilitates combustion reactions. We expect $Al_xO_y^+$ with an even number of aluminum atoms to be more reactive, as these species have an unpaired electron. In agreement with the hypothesis, our calculations reveal that the bond dissociation energy of $Al_xO_yH^+(C_2H_5)$ to form $C_2H_5\cdot$ which is the active species for combustion acceleration, is much smaller for Al_2O^+ and $Al_4O_7^+$ than for $Al_3O_2^+$ and $Al_3O_4^+$. However, some closed-shell species, such as $Al_3O_4^+$, are predicted to be quite reactive and in general, the oxygen-rich clusters have smaller barriers to C-H activation.

Supporting Information

Experimental details; experimental and calculated vibrational spectra of additional isomers; potential energy surfaces for $Al_xO_y^+ + C_2H_6$ reactions; calculated energies, geometries, vibrational frequencies and intensities of key species at the B3LYP/TZVP and B3LYP/6-311+G(d,p) level of theory (with and without local mode Hamiltonian).

Acknowledgements

Financial support from the National Science Foundation under award no. CHE-2154391 is gratefully acknowledged. AP is supported by a Development and Promotion of Science and Technology Talents Project, Thai government scholarship. The authors are grateful for computational resources provided by the Massachusetts Green High-Performance Computing Center (MGHPCC). We thank Prof. Edwin L. Sibert III for the use of his local mode Hamiltonian code. We also acknowledge helpful discussions with Drs. Nicholas Shuman, Shaun G. Ard and Albert Viggiano.

References

[1] Z. Luo, S. N. Khanna, *Metal Clusters and Their Reactivity*, Springer Singapore, Singapore, **2020**.

[2] K. A. Zemski, D. R. Justes, A. W. Castleman Jr., *J. Phys. Chem. B* **2002**, *106*, 6136–6148.

[3] T. Edwards, *J. Propuls. Power* **2003**, *19*, 1089–1107.

[4] C. I. Raţ, A. Soran, R. A. Varga, C. Silvestru, *Adv. Organomet. Chem.* **2018**, *70*, 233–311.

[5] S. Feyel, J. Döbler, D. Schröder, J. Sauer, H. Schwarz, *Angew. Chem. Int. Ed.* **2006**, *45*, 4681–4685.

[6] H. Schwarz, *Angew. Chem. Int. Ed.* **2011**, *50*, 10096–10115.

[7] Z. C. Wang, T. Weiske, R. Kretschmer, M. Schlangen, M. Kaupp, H. Schwarz, *J. Am. Chem. Soc.* **2011**, *133*, 16930–16937.

[8] M. Soustelle, *An Introduction to Chemical Kinetics*, **2011**.

[9] S. P. Venkatesan, P. N. Kadiresh, *Int. J. Appl. Eng. Res.* **2015**, *10*, 5741–5749.

[10] D. Schröder, H. Schwarz, *Angew. Chem. Int. Ed. Engl.* **1990**, *29*, 1433–1434.

[11] Y. X. Zhao, X. N. Wu, Z. C. Wang, S. G. He, X. L. Ding, *Chem. Comm.* **2010**, *46*, 1736–

1738.

[12] K. Chen, Z. C. Wang, M. Schlangen, Y. D. Wu, X. Zhang, H. Schwarz, *Chem. -Eur. J.* **2011**, *17*, 9619–9625.

[13] D. Schröder, J. Roithová, E. Alikhani, K. Kwapien, J. Sauer, *Chem. -Eur. J.* **2010**, *16*, 4110–4119.

[14] H. Schwarz, P. González-Navarrete, J. Li, M. Schlangen, X. Sun, T. Weiske, S. Zhou, *Organometallics* **2017**, *36*, 8–17.

[15] S. Feyel, J. Döbler, R. Höckendorf, M. K. Beyer, J. Sauer, H. Schwarz, *Angew. Chem. Int. Ed.* **2008**, *47*, 1946–1950.

[16] J. Ma, X. Wu, Y. Zhao, X. Ding, S. He, *J. Phys. Chem. A* **2010**, *114*, 10024–10027.

[17] Y. X. Zhao, J. Y. Yuan, X. L. Ding, S. G. He, W. J. Zheng, *Phys. Chem. Chem. Phys.* **2011**, *13*, 10084–10090.

[18] A. Hahma, A. Gany, K. Palovuori, *Combust. Flame* **2006**, *145*, 464–480.

[19] Y. Gan, L. Qiao, *Combust. Flame* **2011**, *158*, 354–368.

[20] V. V. Smirnov, S. A. Kostritsa, V. D. Kobtsev, N. S. Titova, A. M. Starik, *Combust. Flame* **2015**, *162*, 3554–3561.

[21] M. H. G. Prechtl, M. Teltewskoi, A. Dimitrov, E. Kemnitz, T. Braun, *Chem. -Eur. J.* **2011**, *17*, 14385–14388.

[22] S. Biswas, D. Paul, C. He, N. Dias, M. Ahmed, M. L. Pantoya, R. I. Kaiser, *J. Phys. Chem. Lett.* **2023**, *14*, 9341–9350.

[23] L. Zhou, N. Piekiel, S. Chowdhury, M. R. Zachariah, *J. Phys. Chem. C* **2010**, *114*, 14269–14275.

[24] L. Zhou, N. Piekiel, S. Chowdhury, D. Lee, M. R. Zachariah, *J. Appl. Phys.* **2009**, *106*, DOI 10.1063/1.3225907.

[25] K. R. Asmis, *Phys. Chem. Chem. Phys.* **2012**, *14*, 9270–9281.

[26] M. Sierka, J. Döbler, J. Sauer, G. Santambrogio, M. Brümmer, L. Wöste, E. Janssens, G. Meijer, K. R. Asmis, *Angew. Chem. Int. Ed.* **2007**, *46*, 3372–3375.

[27] D. Van Heijnsbergen, K. Demyk, M. A. Duncan, G. Meijer, G. Von Helden, *Phys. Chem. Chem. Phys.* **2003**, *5*, 2515–2519.

[28] X. Song, M. R. Fagiani, S. Gewinner, W. Schöllkopf, K. R. Asmis, F. A. Bischoff, F. Berger, J. Sauer, *J. Chem. Phys.* **2016**, *144*, 244305.

[29] G. Santambrogio, E. Janssens, S. Li, T. Siebert, G. Meijer, K. R. Asmis, J. Döbler, M. Sierka, J. Sauer, *J. Am. Chem. Soc.* **2008**, *130*, 15143–15149.

[30] D. Kiawi, Infrared Studies of Astronomically Relevant Metallic Clusters and Their Interactions with Simple Molecules, PhD Thesis, University of Amsterdam (NL), **2016**.

[31] H. Schwarz, S. Shaik, J. Li, *J. Am. Chem. Soc.* **2017**, *139*, 17201–17212.

[32] N. S. Shuman, S. G. Ard, A. A. Viggiano, *Private Communication*, **2024**.

[33] J. Roithová, *Chem. Soc. Rev.* **2012**, *41*, 547–559.

[34] D. Schröder, H. Schwarz, *Proc. Natl. Acad. Sci. U. S. A.* **2008**, *105*, 18114–18119.

[35] J. Roithova, D. Schröder, *Chem. Rev.* **2010**, *110*, 1170–1211.

[36] Z. C. Wang, N. Dietl, R. Kretschmer, J. B. Ma, T. Weiske, M. Schlangen, H. Schwarz, *Angew. Chem. Int. Ed.* **2012**, *51*, 3703–3707.

[37] M. of Defence, *Defence Standard 91-91: Turbine Fuel, Kerosine Type, Jet A-1 (Amd 3)*, Glasgow, **2011**.

[38] J. N. Harvey, M. Diefenbach, D. Schröder, H. Schwarz, *Int. J. Mass Spectrom.* **1999**, *182–183*, 85–97.

[39] T. Wende, J. Döbler, L. Jiang, P. Claes, E. Janssens, P. Lievens, G. Meijer, K. R. Asmis, J. Sauer, *Int. J. Mass Spectrom.* **2010**, *297*, 102–106.

[40] Z. Deng, X. Lu, Z. Wen, S. Wei, Y. Liu, D. Fu, L. Zhao, W. Guo, *Phys. Chem. Chem. Phys.* **2013**, *15*, 16172–16182.

[41] J. Husband, F. Aguirre, P. Ferguson, R. B. Metz, *J. Chem. Phys.* **1999**, *111*, 1433–1437.

[42] D. W. Rothgeb, J. E. Mann, C. C. Jarrold, *J. Chem. Phys.* **2010**, *133*, 054305.

[43] J. Kozubal, T. Heck, R. B. Metz, *J. Chem. Phys.* **2023**, *159*, 174305.

[44] A. Kocak, G. Austein-Miller, W. L. Pearson, G. Altinay, R. B. Metz, *J. Phys. Chem. A* **2013**, *117*, 1254–1264.

[45] D. Kaur, A. M. de Souza, J. Wanna, S. A. Hammad, L. Mercorelli, D. S. Perry, *Appl. Opt.* **1990**, *29*, 119–124.

[46] I. E. Gordon, L. S. Rothman, C. Hill, R. V. Kochanov, Y. Tan, P. F. Bernath, M. Birk, V. Boudon, A. Campargue, K. V. Chance, B. J. Drouin, J. M. Flaud, R. R. Gamache, J. T. Hodges, D. Jacquemart, V. I. Perevalov, A. Perrin, K. P. Shine, M. A. H. Smith, J. Tennyson, G. C. Toon, H. Tran, V. G. Tyuterev, A. Barbe, A. G. Császár, V. M. Devi, T. Furtenbacher, J. J. Harrison, J. M. Hartmann, A. Jolly, T. J. Johnson, T. Karman, I.

Kleiner, A. A. Kyuberis, J. Loos, O. M. Lyulin, S. T. Massie, S. N. Mikhailenko, N. Moazzen-Ahmadi, H. S. P. Müller, O. V. Naumenko, A. V. Nikitin, O. L. Polyansky, M. Rey, M. Rotger, S. W. Sharpe, K. Sung, E. Starikova, S. A. Tashkun, J. Vander Auwera, G. Wagner, J. Wilzewski, P. Wcisło, S. Yu, E. J. Zak, *J. Quant. Spectrosc. Radiat. Transf.* **2017**, *203*, 3–69.

[47] M. J. Frisch, G. W. Trucks, H. B. Schlegel, G. E. Scuseria, M. a. Robb, J. R. Cheeseman, G. Scalmani, V. Barone, G. a. Petersson, H. Nakatsuji, X. Li, M. Caricato, a. V. Marenich, J. Bloino, B. G. Janesko, R. Gomperts, B. Mennucci, H. P. Hratchian, J. V. Ortiz, a. F. Izmaylov, J. L. Sonnenberg, Williams, F. Ding, F. Lipparini, F. Egidi, J. Goings, B. Peng, A. Petrone, T. Henderson, D. Ranasinghe, V. G. Zakrzewski, J. Gao, N. Rega, G. Zheng, W. Liang, M. Hada, M. Ehara, K. Toyota, R. Fukuda, J. Hasegawa, M. Ishida, T. Nakajima, Y. Honda, O. Kitao, H. Nakai, T. Vreven, K. Throssell, J. a. Montgomery Jr., J. E. Peralta, F. Ogliaro, M. J. Bearpark, J. J. Heyd, E. N. Brothers, K. N. Kudin, V. N. Staroverov, T. a. Keith, R. Kobayashi, J. Normand, K. Raghavachari, a. P. Rendell, J. C. Burant, S. S. Iyengar, J. Tomasi, M. Cossi, J. M. Millam, M. Klene, C. Adamo, R. Cammi, J. W. Ochterski, R. L. Martin, K. Morokuma, O. Farkas, J. B. Foresman, D. J. Fox, **2013**, Gaussian 09, Revision D.01, Gaussian, Inc.

[48] E. L. Sibert III, D. P. Tabor, N. M. Kidwell, J. C. Dean, T. S. Zwier, *J. Phys. Chem. A* **2014**, *118*, 11272–11281.

[49] D. P. Tabor, D. M. Hewett, S. Bocklitz, J. A. Korn, A. J. Tomaine, A. K. Ghosh, T. S. Zwier, E. L. Sibert III, *J. Chem. Phys.* **2016**, *144*, 224310.

[50] A. Armstrong, H. Zhang, A. C. Reber, Y. Jia, H. Wu, Z. Luo, S. N. Khanna, *J. Phys. Chem. A* **2019**, *123*, 7463–7469.

[51] H. Schwarz, *Isr. J. Chem.* **2014**, *54*, 1413–1431.

[52] M. R. Fagiani, X. Song, S. Debnath, S. Gewinner, W. Schöllkopf, K. R. Asmis, F. A. Bischoff, F. Müller, J. Sauer, *J. Phys. Chem. Lett.* **2017**, *8*, 1272–1277.

[53] T. Shimanouchi, *Tables of Molecular Vibrational Frequencies, Consolidated Volume I*, National Bureau Of Standards, Gaithersburg, MD, **1972**.

[54] J. C. Marcum, R. B. Metz, *J. Phys. Chem. A* **2023**, *127*, 5091–5103.

[55] F. Müller, J. B. Stückrath, F. A. Bischoff, L. Gagliardi, J. Sauer, S. Debnath, M. Jorewitz, K. R. Asmis, *J. Am. Chem. Soc.* **2020**, *142*, 18050–18059.

[56] R. G. Gilbert, S. C. Smith, *Theory of Unimolecular and Recombination Reactions*, Blackwell Scientific Publications, Oxford, **1990**.

[57] M. A. Ashraf, Spectroscopic Studies of Gas-Phase Metal Cation Complexes with Alkanes and Ammonia, PhD Thesis, University of Massachusetts Amherst (US), **2018**.

[58] B. Xu, Y. X. Zhao, X. N. Li, X. L. Ding, S. G. He, *J. Phys. Chem. A* **2011**, *115*, 10245–10250.

[59] M. Perera, K. M. Roenitz, R. B. Metz, O. Kostko, M. Ahmed, *J. Spectrosc. Dyn.* **2014**, *4*, 21.